NASA-CR-193123

Old Dominion University Research Foundation

DEPARTMENT OF MECHANICAL ENGINEERING & MECHANICS
COLLEGE OF ENGINEERING & TECHNOLOGY
OLD DOMINION UNIVERSITY
NORFOLK, VIRGINIA 23529

LARGE ANGLE MAGNETIC SUSPENSION TEST FIXTURE

By

Colin P. Britcher, Principal Investigator

Progress Report
For the period November 1, 1992 to May 31, 1993

Prepared for
National Aeronautics and Space Administration
Langley Research Center
Hampton, Virginia 23681-0001

Under
Research Grant NAG-1-1056
Nelson J. Groom, Technical Monitor
GCD-Spacecraft Controls Branch

June 1993

DEPARTMENT OF MECHANICAL ENGINEERING & MECHANICS
COLLEGE OF ENGINEERING & TECHNOLOGY
OLD DOMINION UNIVERSITY
NORFOLK, VIRGINIA 23529

LARGE ANGLE MAGNETIC SUSPENSION TEST FIXTURE

By

Colin P. Britcher, Principal Investigator

Progress Report
For the period November 1, 1992 to May 31, 1993

Prepared for
National Aeronautics and Space Administration
Langley Research Center
Hampton, Virginia 23681-0001

Under
Research Grant NAG-1-1056
Nelson J. Groom, Technical Monitor
GCD-Spacecraft Controls Branch

Submitted by the
Old Dominion University Research Foundation
P.O. Box 6369
Norfolk, Virginia 23508-0369

June 1993

INTRODUCTION

This brief report will review the progress made under the subject Grant in the period 11/1/92 - 5/31/93. The research involves the continued development of the Large Angle Magnetic Suspension Test Fixture (LAMSTF) and also the recommissioning of an additional piece of exisiting hardware.

REVIEW OF CURRENT AND ONGOING WORK

During the period in question, the initial configuration of LAMSTF was completed and made routinely and reliably operational. A digital phase advance controller was completed and documented. The goal of a controlled 360^{o} rotation was been achieved. Work started on the recommissioning of the Annular Suspension and Pointing System (ASPS). A more detailed breakdown of work completed follows :

(i) Modelling. A series of simplified eddy current measurements have been made which show promise in resolving the related dynamic modelling problem. A new version of the computer code GFUN has been supplied and has been installed and tested on the SCB SUN network.

(ii) Position sensing. Design work was started on a revised optical system, intended to overcome continuing difficulties is establishing and maintaining calibration of the existing system and also to incorporate roll sensing.

(iii) Controller. The digital controller previously developed under this Grant is presently based on 486-class PC hardware, implementing classical dual phase-advance compensators. Preliminary documentation has been provided.

(iv) Support of the Second International Symposium on Magnetic Suspension Technology. Calls for papers and exhibits were prepared and distributed. Submitted Abstracts were reviewed and author kits sent.

(v) Recommissioning of the Annular Suspension and Pointing System. The hardware has been uncrated, inventoried, positioned in a laboratory and reviewed for condition and ease of recommissioning. Studies of the modifications required to permit suspension in a full gravity field and a review of the control problems have been completed. Copies of the student project papers generated are attached as Appendices to this report. It was concluded that simple shims added to the pole faces would greatly increase the force capability and easily permit suspension in a gravity field. The

increase the force capability and easily permit suspension in a gravity field. The fabrication of the pole shims required to permit such suspension is underway.

PROBLEM AREAS

GFUN has continued to be a rather troublesome code, although the SUN version does execute considerably faster than the previous VAX version and has much superior graphics. The current graduate research assistant, Lucas Foster, is becoming proficient with the code.

PUBLICATIONS DURING THE CURRENT GRANT PERIOD

Groom, N.J.; Britcher, C.P.: A Description of a Laboratory Model Magnetic Suspension System with a Large Angular Capability. 1st IEEE Conference on Control Applications. Dayton, OH, September 1992.

Groom, N.J.; Britcher, C.P.: Stability Considerations for Magnetic Suspension Systems with Electromagnets Mounted in a Planar Array. NASA TP-3229, December 1992.

Ghofrani, M.: Approaches to Control of the Large Angle Magnetic Suspension Test Fixture. NASA CR-191890, December 1992.

Appendix A

"Introduction to Magnetic Bearings"

- A Review of ASPS Modifications for use in a Gravity Field

Lori Skowronski and Anne Bisese
Department of Electrical and Computer Engineering

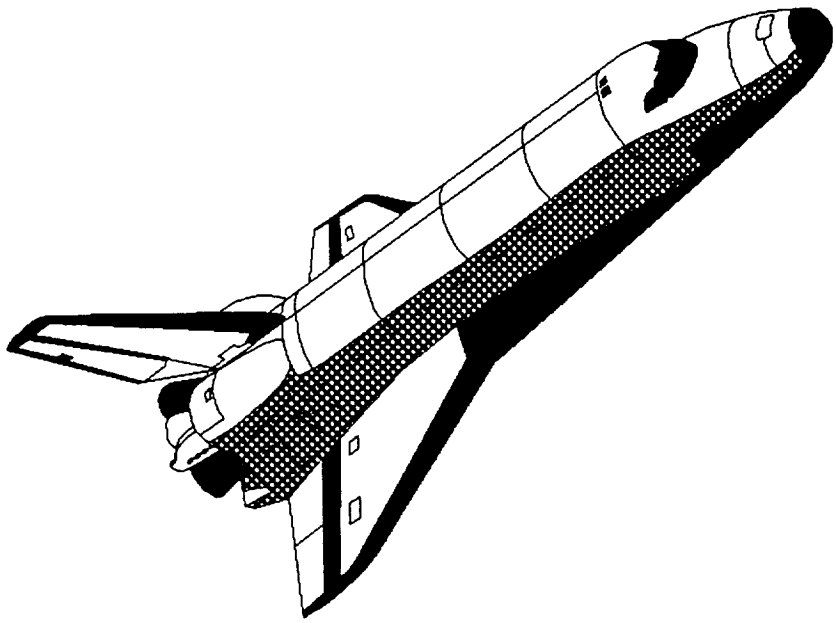

INTRODUCTION TO MAGNETIC BEARINGS

LORI SKOWRONSKI
ANNE BISESE

ECE 485
5 APRIL 1993

INTRODUCTION

Levitation, as far as this report is concerned, is the act of holding up an object with no visible support by means of electromagnetic suspension techniques. Since the 1930's there has been research in single axis suspensions utilizing a magnetic bearing station as shown in Figure 1.

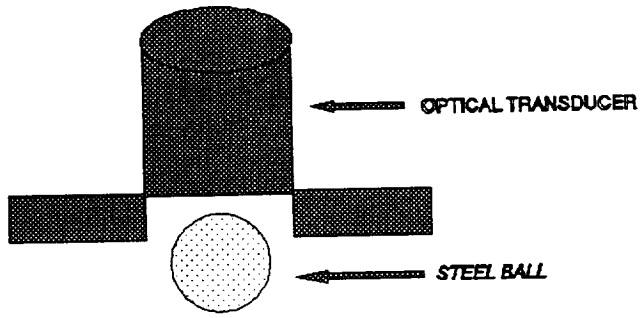

SINGLE MAGNET SUSPENSION

FIGURE 1.

This research has blossomed into the idea of multi-axis suspensions. Multi-axis suspension has several advantages over single axis system, in that it provides control of an object with precision in two or three orthogonal axes. In this report, we discuss the primary use of magnetic-bearing suspension and it's

relevance to what was formally known as NASA's Annular Suspension and Pointing System (ASPS). This system is an experimental pointing system with applications for the space shuttle and the space station programs.

The objectives behind this magnetic suspension research project are to provide insight to the use of the ASPS configuration, to control the solar panels of the space station. This is important to maintain the correct position of the panels in relation to the sun and orbiting space station for the continuous supply of solar energy. Since the panels are suspended, they can be aligned with minimum outside interference. The approach of using magnetic suspension technology guarantees mechanical isolation since there are no contacting surfaces. This isolation reduces vibration transmission and mechanical wear which in turn extends the life of the payload and of the carrier. It should be noted that ASPS has a high pointing accuracy along the line of 0.01 arc-second.

This research will be done in a laboratory setting by incorporating five bearing stations and one motion control station (See Figure 2). We will attempt to suspend an object of dead weight similar to that of a solar panel. The long term applications may include deep-space navigation, fire control in weapon systems, and an improved mass transit system.

THEORY

The principle behind electromagnetic suspension in this project is simply explained by magnetic flux theory. The magnetic flux through any closed figure is the product of the area by the average component of magnetic induction normal to the area. Flux (Φ) is defined by :

$$\Phi = k \int_s B \, dS$$

where k is the constant of proportionality between field and flux density (B). This application can be expanded to represent the principles surrounding single axis suspension. An object is supported, against the force of gravity, by an electromagnet in which the current is controlled electronically in response to a position signal. From Earnshaw's Theorem, it is known that the stability of the system is dependent upon the feedback of this position signal because without control of the current it is fundamentally unstable. To achieve stable suspension, it is necessary to regulate the current in the electromagnet using position feedback of the object to be suspended.

The force of attraction between two objects is given by the formula, $F_m = B^2 \div 2\mu_o$ * Area, where B represents the magnetic flux density, μ_o is permeability of free space, and the area is represented by the cross-sectional area of one pole. This formula comes from the derivation of Maxwell's stress formula. The

electromagnets used in suspension systems are under the influence of an "air gap". The air gap denotes a gap left in the magnetic material; a short gap is usually left in the core material to prevent saturation of the magnetic material by the dc current. This implies the gap flux density is directly proportional to the ampere turns "NI" and inversely proportional to the length "g", gap length. The formula then becomes, $F_m = (1/2\mu_o) * (\mu_o * NI/g)^2 *$ Area, as seen by the following derivation.

$$NI = \sum_m H_m l_m$$

where H_m is the magnetic field and l_m is the length of the material.

Maxwell's equation states: $H = \frac{B}{\mu}$ $\therefore$ $NI = \sum_m \frac{B_m}{\mu} l_m$

so, $NI = \frac{B_i}{\mu_i} l_i + \frac{B_a}{\mu_a} l_a$

the first term goes away because $\mu_i \gg \mu_a$

$\therefore$ $\frac{B_a}{\mu_a} l_a$ dominates

so, $NI = \frac{B_a}{\mu_a} l_a$ $\mu_a = \mu_{air} = \mu_o$

for this configuration ------l_a = 2G.W. = g,

substitute into the equation, $B = B_{air}$

$$\therefore \quad NI = \frac{B_{air}}{\mu_o}(g) \qquad \text{solving for } B_a$$

$$B_{air} = \frac{NI\ \mu_o}{g}$$

The governing equation states : $F_m = \frac{B^2}{2\mu_o}\ Area$

$$F_m = \frac{[\frac{NI\ \mu_o}{g}]^2\ Area}{2\mu_o}$$

$$F_m = \frac{(NI)^2\ \mu_o^2\ Area}{2g^2\ \mu_o}$$

$$F_m = \frac{(NI)^2\ \mu_o\ Area}{2g^2}$$

However, in this system we have A = 2*(width*length), as with the air gap, taking into account two pole faces.

$$\therefore \quad F_m = \mu_o \frac{(NI)^2}{g^2}\ Area$$

The implication of this gap distance is dependent upon several separate factors, the weight of the suspended object, the induced current, and number of turns on the coil. (See Figure 3)

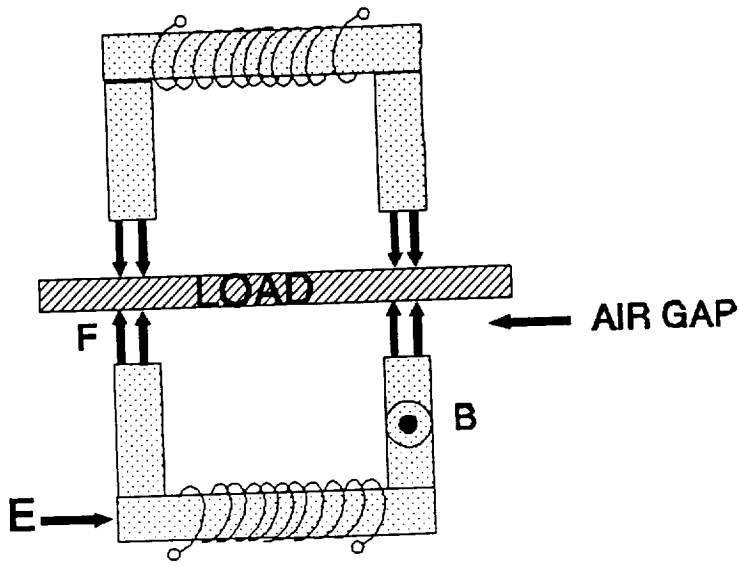

Figure 3

With a single axis suspension system it is obvious to see that there is only one position on the vertical axis at which the magnetic lift force is equal to the weight of the object. Any deviation to this position will result in the object's displacement.

The translation motion of a free body in space will have three degrees of freedom associated with it as well as three degrees of freedom relating to rotational motion. Again, based upon the classical force equations, the motion equations can be derived for this multi-bearing system. The motion of the system can then be described by six non-linear second order differential equations. The non-linearity could be due to bearing characteristics and/or rotations due to angular momentum. The equations can be linearized

after utilizing Maxwell's stress formula to find the magnetic stress tensor. The resulting matrix of the tensor provides values for all components of magnetic stress along each of the coordinate axes. The rigid body force acting on an object is obtained by integrating these components over its bounding surface. As far as the rotation due to angular momentum is concerned, a summation of the moments is calculated and then linearized. It should be noted that for efficient operation of suspension systems utilizing dc magnets, small air gaps which can be precisely controlled are required.

In complicated systems such as the ASPS, multiple bearing stations are utilized. There are several difficulties associated with multi-magnetic systems to include the management of six separate air-gaps. The integrated control portion will be addressed in a separate report.

DESIGN APPROACH

Using the related force equation, $F = \mu_o \div [(NI)^2 \div g^2]$ **Area, we are to modify the existing multi-bearing system to meet the new requirements assigned. From the design documentation, the weight of the rotor was given as 47.6 lbs or approximately 211.7N. This implies that each bearing station should support 16 lbs or 71.2N. However, to allow for errors and possible addition of payload weight, a 1.3 safety factor is incorporated. Each station should hold 20.63 lbs or a force of 91.75N. An additional factor of 1.5 is included, for control purposes, to give a sum total of 30.94 lbs or 137.63N per axial station. This 1.5 factor is the peak force prior to saturation of the magnetic material. Since the axial magnetic bearing station can hold twice the amount as the radial bearing station, we chose to redesign the axial station first in order to get a reasonable approach to the new requirements. In the formula above, there are five variables that can be changed. Systematically we selected the variable to be altered and made the appropriate calculations.*

In the first design, we regarded the $(NI)^2$ *term to be a single factor and the only variable to be considered while all the others were held constant from the original design specifications. This calculation indicated that the "NI" term had to be increased by 54.5% to meet the required specifications. The "NI" term can be broken into it's two components, one involving current and the other number of turns. The number of turns would be very difficult*

to increase due to the replacement of the entire coil and the protective coating on the wire. Since it would not be cost effective to increase the number of turns, the alternative is to increase the current. This also is not feasible because increasing the current will cause other problems in the system. These include overheating of the bearings, melting of the wire, and magnetic material saturation. The comparison of the original and new design specifications are shown in Table 1 and Graph 1. The only advantage of this approach would be that the force would increase substantially since $F \propto (NI)^2$.

In the second design, we regarded the area to be a single factor. To meet the new specifications, the area was calculated to be 1.4E-3 square meters and an increase of 79.3% as shown in Table 1 and Graph 2. We took into consideration an increase in length, width, and a combination of both dimensions. This approach was again not feasible due to cost constraints. It would be very expensive to rebuild the bearing station magnet to meet the new specifications.

The third design took into consideration the gap width. The original specifications set the nominal gap width to be approximately 6.35mm and at the time of this research this was an acceptable distance. Since that time, small-air gap theory, commonly used for magnetic bearing for machinery, has decreased the gap distance to 1/100 of an inch. This new concept led us to the conclusion that the movement of the bearing to decrease the gap width would be the most cost effective and easiest design change.

Taking in to consideration the original design specs and keeping all variables constant, we calculated the gap width to be approximately 3.466mm which is a 83% decrease in distance (see Table 1 and Graph 3). If this decrease should cause saturation or over heating problems, the other design variables will have to be altered. In the testing portion of this report, it is shown that there was no overheating or saturation due to the change in the gap width.

The radial bearing station designs will be minimally modified because the translational motion is negligible. From the original design, we determined that the variables could remain constant with the same change in gap width as the axial bearings.

TABLE 1.

	ORIGINAL	DESIGN	% CHANGE
N--# OF TURNS	2148	4720	+54.5
I--CURRENT	1.4	2.2	+36.4
A--AREA	$2.90X10^{-4}$ m^2	$1.40X10^{-3}$ m^2	+79.3
g--GAP WIDTH	6.35mm	3.47mm	-83.0

Graph 1

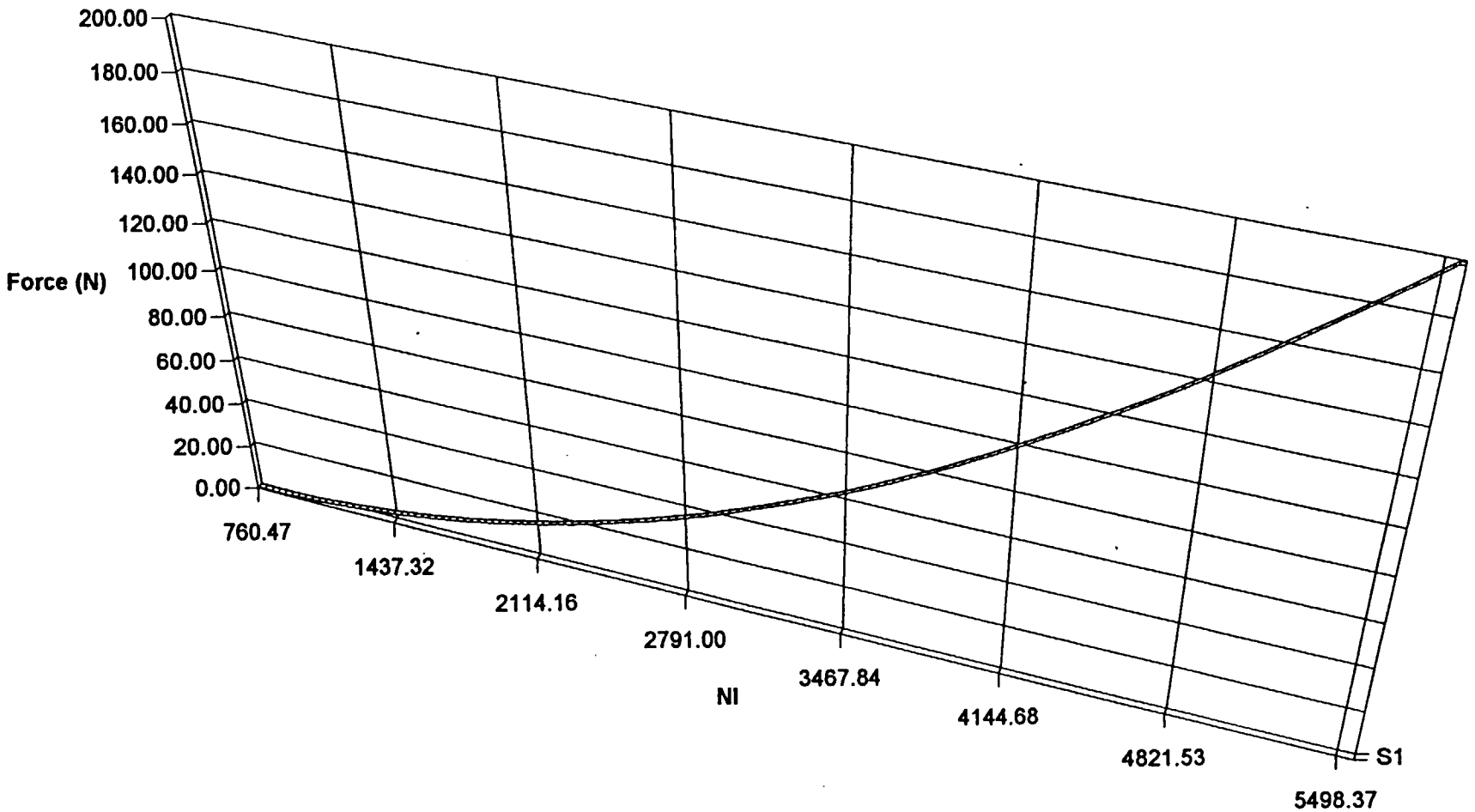
200.00
180.00
160.00
140.00
120.00
100.00
80.00
60.00
40.00
20.00
0.00
Force (N)
760.47
1437.32
2114.16
2791.00
3467.84
4144.68
4821.53
5498.37
NI
S1

Graph 2

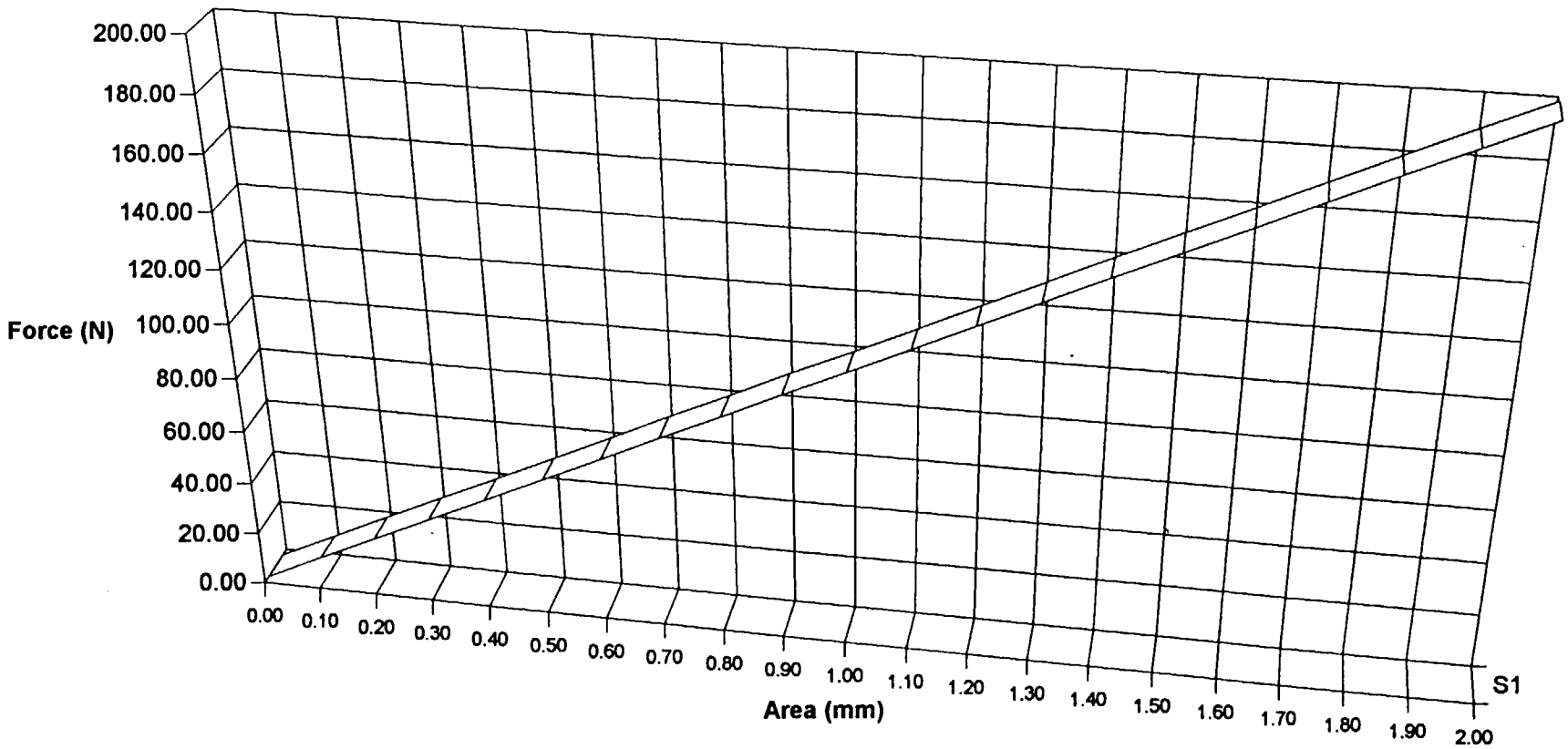
Force (N)
200.00
180.00
160.00
140.00
120.00
100.00
80.00
60.00
40.00
20.00
0.00
0.00
0.10
0.20
0.30
0.40
0.50
0.60
0.70
0.80
0.90
1.00
1.10
1.20
1.30
1.40
1.50
1.60
1.70
1.80
1.90
2.00
Area (mm)
S1

Graph 3

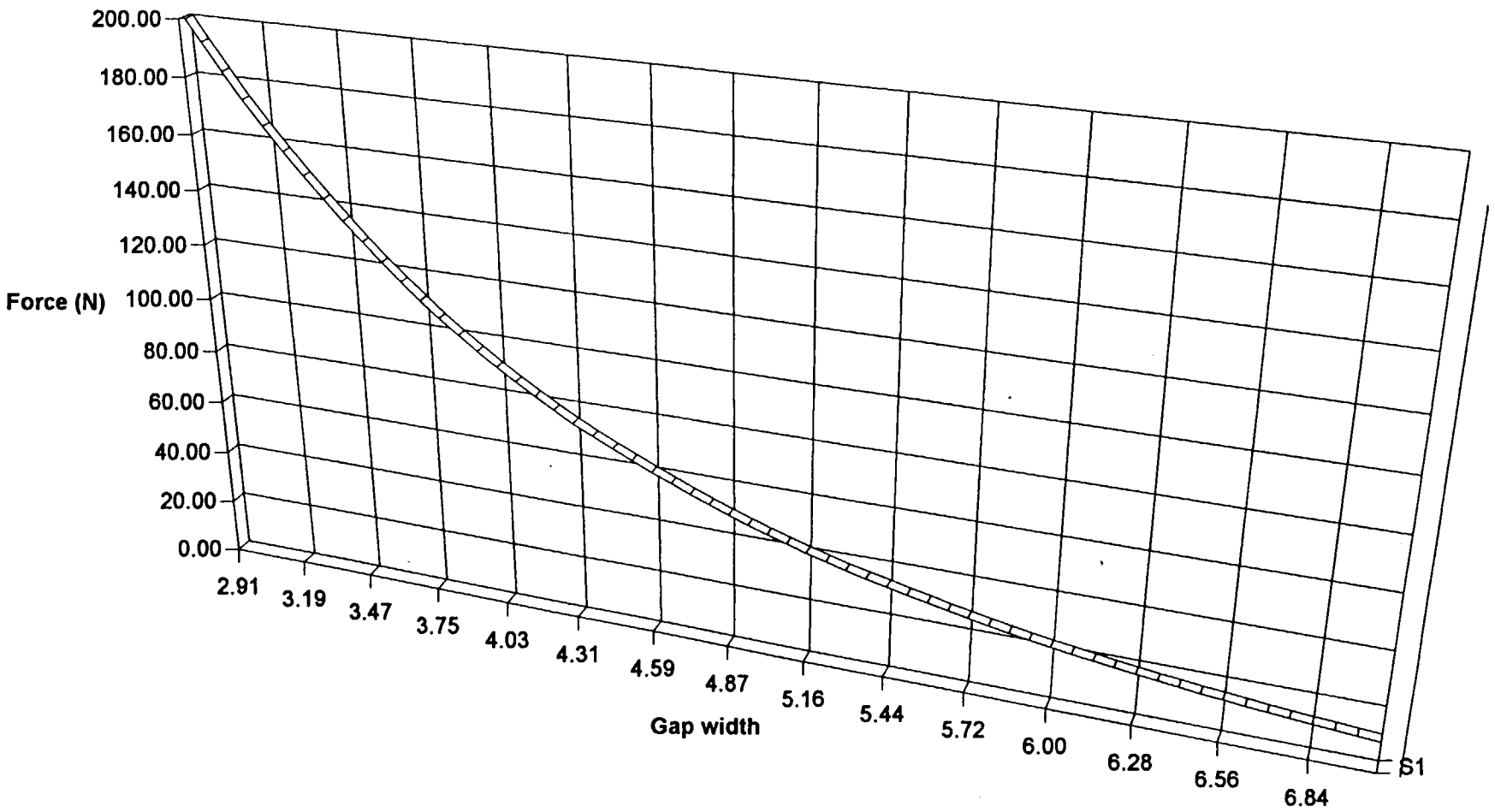
200.00
180.00
160.00
140.00
120.00
100.00
80.00
60.00
40.00
20.00
0.00
Force (N)
2.91
3.19
3.47
3.75
4.03
4.31
4.59
4.87
5.16
5.44
5.72
6.00
6.28
6.56
6.84
Gap width
S1

TESTING AND DESIGN EVALUATION

The original ASPS design and testing was accomplished in the mid 1970's to the early 1980's. Since that time, the ASPS program has been on hold. The purpose of this experimentation is to verify the operational capability of the rotor assembly under new design constraints.

In the new design, the gap width was decreased to increase the lift capabilities. As mentioned in the design section, saturation of the material and overheating of the coils could be two problems encountered by decreasing the gap width. A mathematical exercise can be used to prove the material does not saturate. Knowing that the flux is a constant through out the circuit, flux density in the smallest cross-sectional area can be calculated. The following calculations will show that saturation should not be a problem with the new design.

From previous derivation:

$$B_a = \frac{(NI)\ \mu_o}{2g} = 0.389\ Tesla$$

$$\Phi = constant = B_a A_a = B_i A_i$$

$$\therefore\ B_i = \frac{A_a}{A_i} B_a$$

A_i will be the smallest cross-sectional area, which will yield the largest "B"; this will show that saturation does not occur.

A_a = 1.55E-3 A_i = 7.76E-4 B_a = .389T

$$B_i = \frac{1.55E-3}{7.76E-4} \ (0.389T) = 0.78T$$

As shown in Figure 4, B_{sat} for the material is given as 1.6T. The B_{bias} was calculated as .4T and the "B" for the smallest cross-sectional area is .8T, which is well below the B_{sat} level. There should be no saturation problems due to the new gap width.

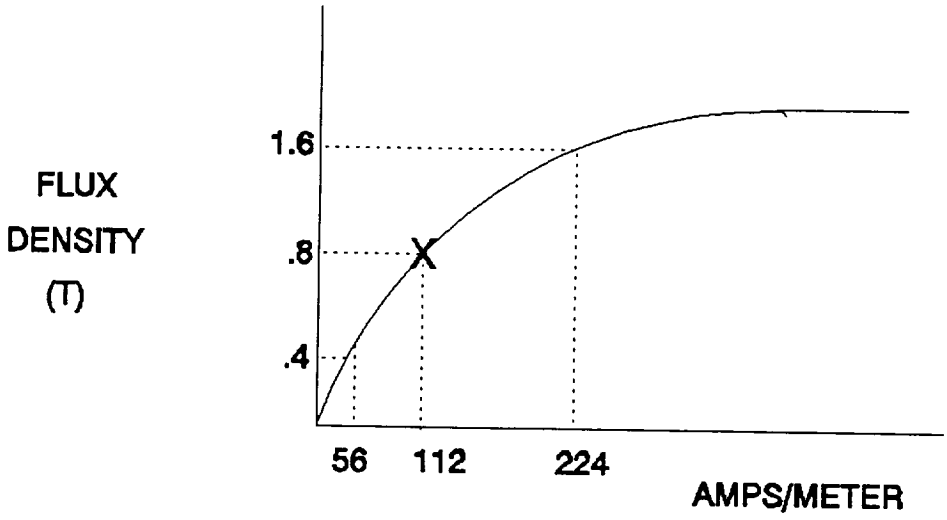

The second consideration mentioned was the overheating of the coils. This was proven in the lab by running a current of 1.5 amps through the coils for twenty minutes. A thermocoupler

was connected to the outside casing of the coil and a piece of foam rubber was positioned around both to insulate them from the outside air. As seen in Graph 4, the increase in temperature was minimal. The current was increased to 2 amps and another twenty minute test of time versus temperature was performed. Graph 5 indicates the increase in temperature was again minimal.

Each of the bearing stations were tested for their magnetic force by using a 1.5 amp current and a magnetic sensing devise. This proves the magnets are in operating condition.

From these three simple experiments, we believe that our design will function as desired under the specific design criteria.

The actual testing of the rotor assembly was accomplished by the following steps:

1) The schematics indicated the power to the axial bearing stations came from plug J402. Each bearing station is designated by either A, B, or C with pins 1, 9, and 20 being the input and 2, 10, and 21 being the output. To have each bearing station operating simultaneously, the output of A-pin 2 was connected to the input of B-pin 9 and B-pin 10 was connected to C-pin 20. A-pin 1 was connected to the power supply and C-pin 21 was connected to the return.

2) To obtain the appropriate current, two power supplies were connected in series. It should be noted that with them connected in series, the current was monitored by an external amp meter to insure the exact current. We adjusted

the current to approximately 1.6 amps and manually lifted the rotor until it was magnetically held by the top portion of the bearing assembly. We then decreased the current at 0.01 increments until the rotor released itself at approximately 1.35 amps.

3) The desired air gap was maintained by inserting a non-magnetic material (aluminum) shim to simulate an air gap of 3.46 millimeter. Therefore, when the rotor was raised, the assembly was operating at the designed criteria. The results are shown in the accompanying photographs.

Table of Temperature (C) Increase

Time (Minutes)	0.00	1.00	2.00	3.00	4.00	5.00	6.00	7.00	8.00	9.00	10.00	11.00	12.00	13.00	14.00	15.00	16.00	17.00	18.00	19.00	20.00
Graph 4																					
Actual	23.60	24.20	25.40	26.60	27.80	28.80	29.60	30.60	31.40	32.00	32.80	33.20	34.00	34.40	35.00	35.60	35.60	35.60	37.00	37.00	38.00
Theoretical	23.60	24.39	25.18	25.96	26.75	27.54	28.33	29.12	29.91	30.69	31.48	32.27	33.06	33.85	34.64	35.42	36.21	37.00	37.79	37.79	37.79
Graph 5																					
Actual	23.60	24.40	26.60	29.20	31.60	33.80	35.80	37.60	39.40	41.00	42.80	44.40	45.80	47.20	48.60	49.60	51.00	52.20	53.20	54.00	55.00
Theoretical	23.60	25.34	27.08	28.82	30.56	32.31	34.05	35.79	37.53	39.27	41.01	42.75	44.49	46.24	47.98	49.72	51.46	53.20	54.94	54.94	54.94

Graph 4

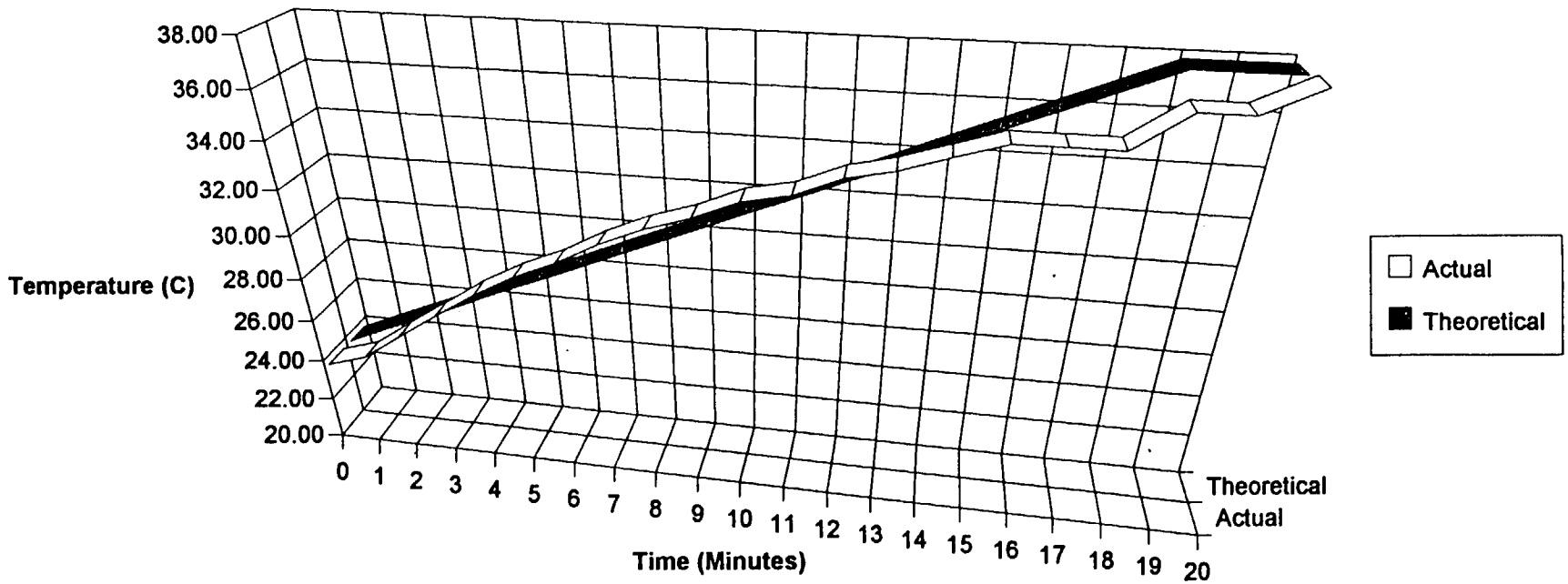
38.00
36.00
34.00
32.00
30.00
28.00
26.00
24.00
22.00
20.00
Temperature (C)
0 1 2 3 4 5 6 7 8 9 10 11 12 13 14 15 16 17 18 19 20
Time (Minutes)
Theoretical
Actual
Actual
Theoretical

Graph 5

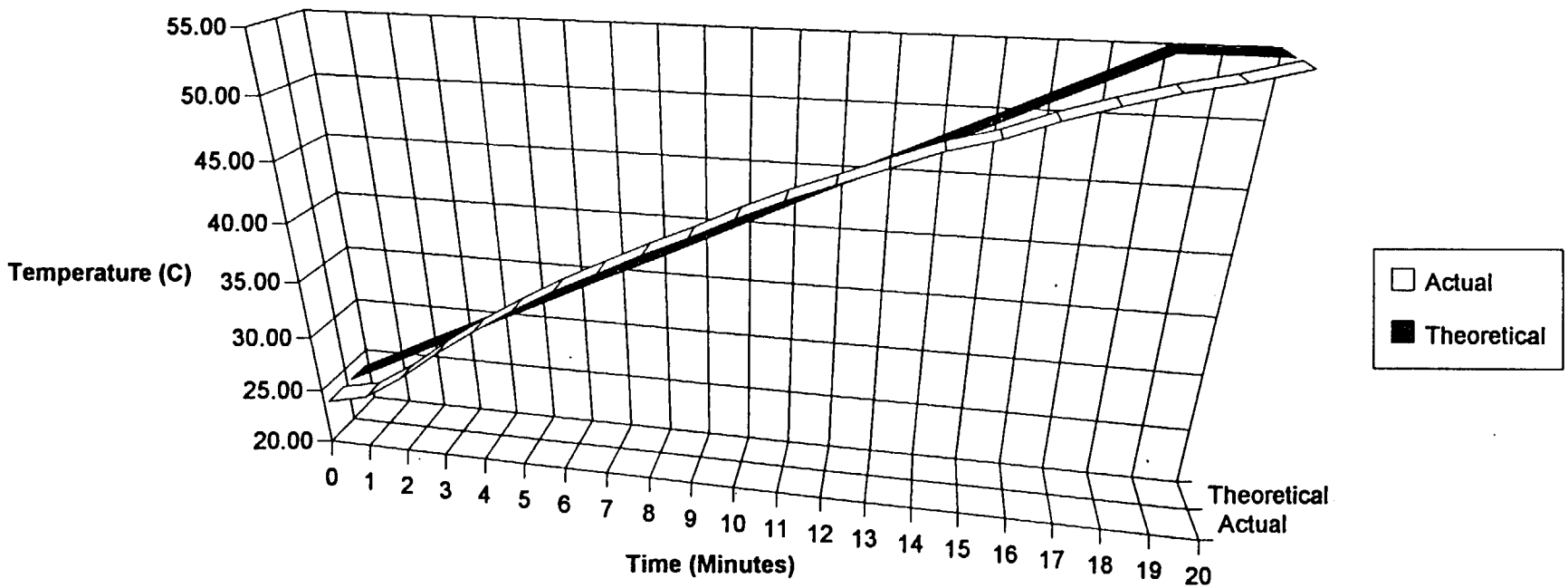
55.00
50.00
45.00
40.00
35.00
30.00
25.00
20.00
Temperature (C)
0 1 2 3 4 5 6 7 8 9 10 11 12 13 14 15 16 17 18 19 20
Time (Minutes)
Theoretical
Actual
Actual
Theoretical

CONCLUSION

Based on the design calculations, the assembly operated within acceptable limits. The current designed for was 1.4 amps, however, the assembly operated correctly at 1.35 amps. This indicates that the assembly could operate at lower currents and also implies there would be no problem with overheating of the coils or saturation of the magnetic material.

The follow-up research for the magnetic bearing system should include integration of the roll-motor assembly with the findings of this report. This would give control of the entire bearing system to roll-motor assembly instead of the few pins referenced in the experimental section of this report. A computer program could be used in conjunction with the control motor for ultimate control of the system.

REFERENCES

1) *International Symposium on Magnetic Suspension Technology, NASA Conference Publication 3152 Part 1.*

2) *B. V. Jayawant, Electromagnetic Levitation and Suspension Techniques.*

3) *Robert R. Humphris, Introduction to Magnetic Bearings*

4) *The Development of the ASPS Vernier System, Final Report, Sperry Corporation.*

5) *ASPS--Final Design Review, Sperry Corporation.*

6) *G. F. Franklin, J. D. Powell, A. Emami-Nasini, Feedback Control of Dynamic Systems.*

7) *F. T. Holmes, Axial Magnetic Suspensions, Physics Review.*

8) *A. T. Carmichael, S. Hinchliffe, P. N. Murgatroyd, I. D. Williams, Magnetic Suspension Systems with Digital Controllers, Review of Scientific Instruments, Aug. 1986.*

9) *M. B. Scudiere, R. A. Willems, G. T. Gillies, Digital Controller For A Magnetic Suspension System, Review of Scientific Instruments, Aug. 1986.*

10) *R. G. Lerner, G. L. Trigg, Encyclopedia of Physics.*

11) *D. M. Considine, Van Nostrand's Scientific Encyclopedia.*

12) *L. Chi Shen, J. Au Kong, Applied Electromagnetism.*

Appendix B

"Annular Suspension and Pointing System

with Controlled DC Elctromagnets"

Josephine L. Vu and Kwok Hung Tam
Department of Electrical and Computer Engineering

Annular Suspension and Pointing System with Controlled DC Electromagnets: ECE 485 Senior Design Project Report

by

Josephine Lynn, Vu, and Kwok Hung, Tam,

Student, Old Dominion University.

Submitted to

Dr. Vahala and Dr. Britcher,

Instructors, Old Dominion University.

April 22, 1993

Pledge:

Tam, Kwok Hung

Josephine L. Vu

Table of contents

Illustrations

List of Symbols

A: cross-sectional area of one side of the actuator

a: assigned constant

B: magnetic flux density in the gap

Bm: magnetic flux density inside the actuator

b: assigned constant

c^2: assigned constant

F(x,i):attractive force between the actuator and the rim(suspended mass)

$G_p(s)$: plant dynamic equation or open loop transfer function

g_1, g_2, g: gap distance

g_o: equilibrium distance

I: input current of the actuator

I_b, I_o: equivalent bias current

i: controlled current

L: inductance of the actuator

L_c: inductance of the coil

L_1: inductance of the gap

l: the length of actuator

m: mass of the rim(suspended mass)

N: number of turns of he coil

R: actuator resistance

s: Laplace transform variable

V: input voltage of the actuator

V_b: equivalent bias voltage

v: controlled voltage

x: controlled distance or small perturbation distance from

equilibrium

μ : permeability of the actuator material

μ_c :permeability of free space

ϕ : magnetic flux

L.H.P : left half plane

ASPS : Annular Suspension and Pointing System

I. Introduction

A. Problem Definition

Frictionless electromagnetic suspension and levitation has attracted much attention since 1970. Applications include high-speed machine tool spindles, ultra-centrifuges, high vacuum pumps, and fly-wheels for energy storage. Methods of producing electromagnetic suspension and levitation include controlled DC electromagnets, diamagnetic materials, superconductors, hybrid systems, and tuned LCR circuits. A comprehensive review lecture of electromagnetic suspension and levitation techniques can be found in reference 1.

The technique of suspension and levitation with controlled DC electromagnets is the most advanced and successful at this time. Many investigations are underway worldwide. Advanced ground transportation schemes, contactless bearings for ultra-high speed, and gyroscopes have been successfully demonstrated by many groups of researchers.[1]

The Annular Suspension and Pointing System (ASPS) developed by the Flight System division of Sperry Corporation[1] is a six-degree of freedom payload pointing system designed for use with the space shuttle. This magnetic suspension and pointing system provides precise controlled pointing in six-degrees of freedom, isolation of payload-carrier disturbances, and end mount controlled pointing. Those are great advantages over the traditional mechanical joints for space applications. More detail discussions of the magnetic suspension joints and mechanical joints can be found in reference

2.

Figure 1 and 2 show the ASPS designed by Sperry Corporation. It consists of six actuators, three for vertical movements, two for radial movements, and one for tangential movements. By the coupling and decoupling matrices (figure 3) [2], we can carefully decompose the command signal of each degree of freedom to each actuator individually. In other words, the coupling and decoupling matrices change the six-degree of freedom ASPS control system to six single-degree of freedom ALPS control systems. Hence, we can design each control loop separately.

figure 1.

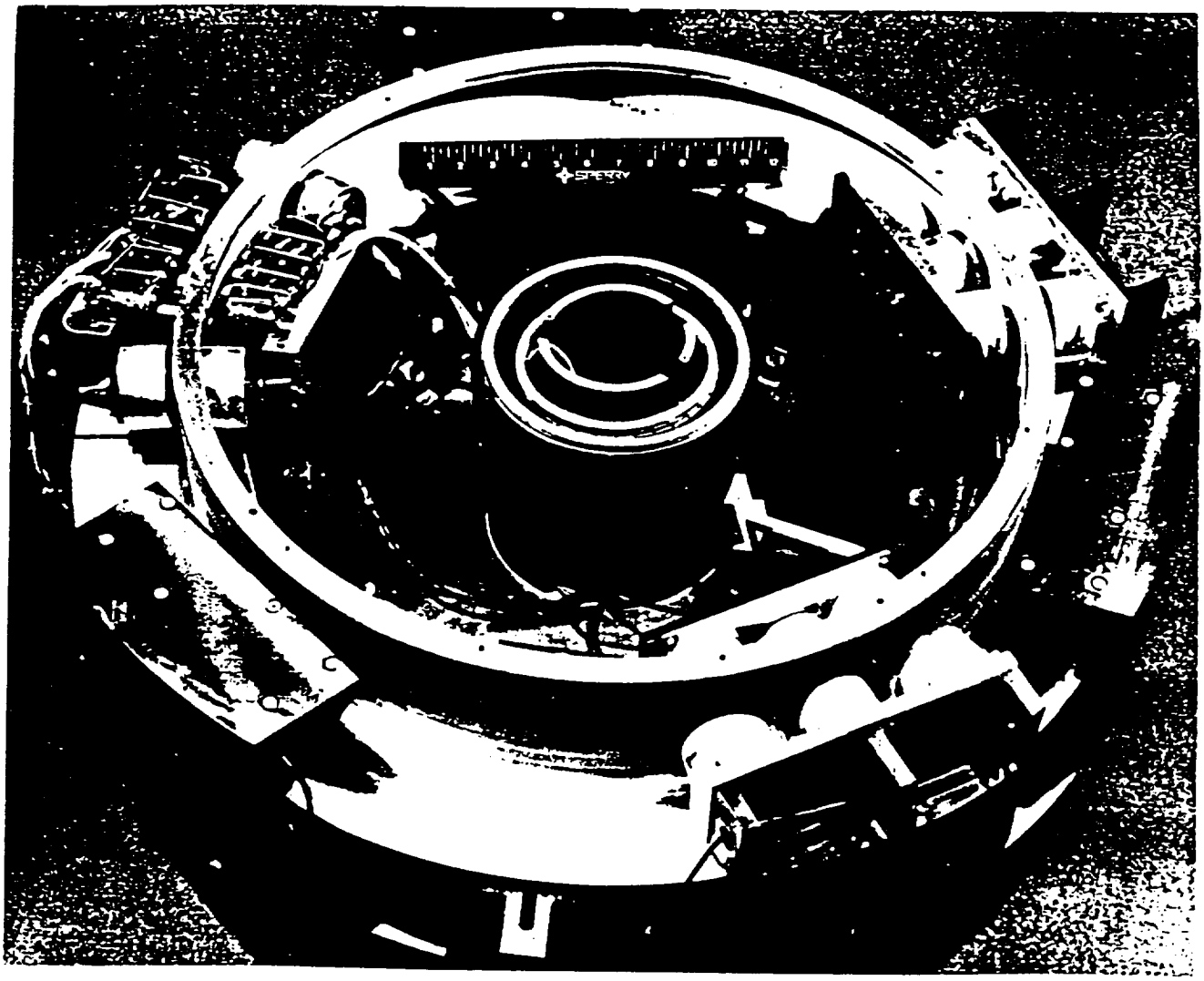

figure 2.

VERNIER ACTUATOR FORCES AND MOMENTS

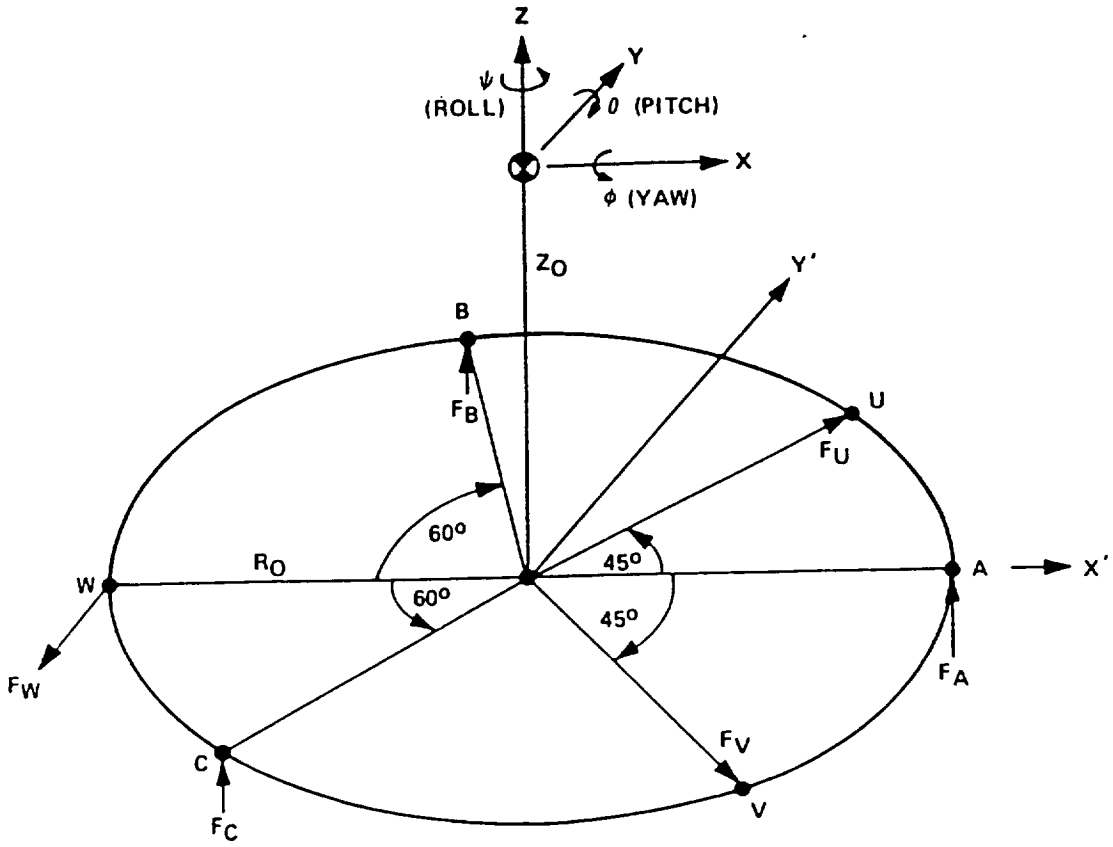

$F_X = F_U \cos 45^\circ + F_V \cos 45^\circ$

$F_Y = F_U \sin 45^\circ - F_V \sin 45^\circ - F_W$

$F_Z = F_A + F_B + F_C$

$T\phi = F_B R_O \sin 60^\circ - F_C R_O \sin 60^\circ + F_U Z_O \sin 45^\circ - F_V Z_O \sin 45^\circ - F_W Z_O$

$T\theta = -F_A R_O + F_B R_O \cos 60^\circ + F_C R_O \cos 60^\circ - F_U Z_O \cos 45^\circ - F_V Z_O \cos 45^\circ$

$T\psi = F_W R_O$

VERNIER ACTUATOR DECOUPLING

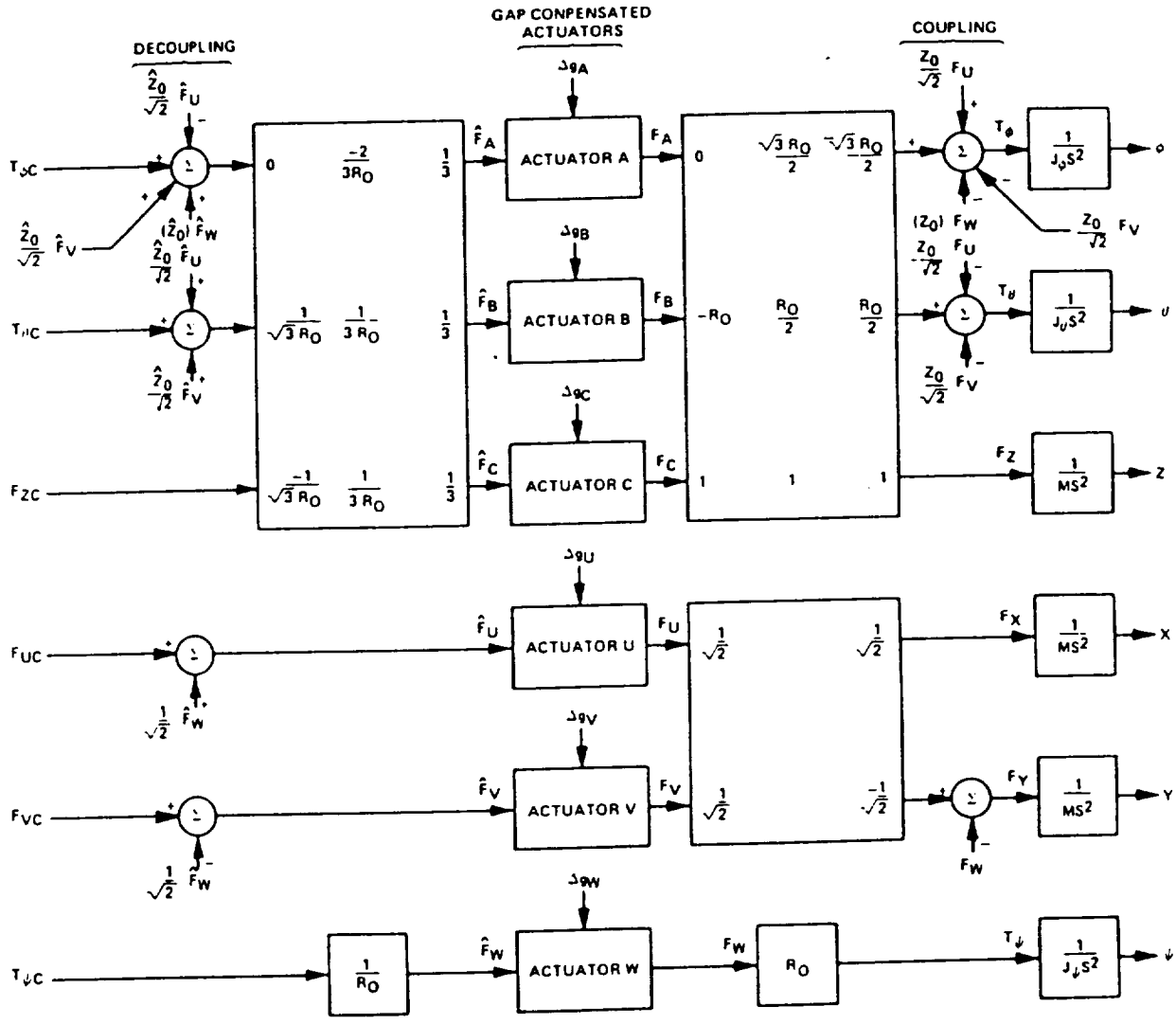

FIGURE 3

B. Project Objectives

(i) Understanding the existing ASPS in the lab.

(ii) Model the dynamics of a single DC controlled ALPS actuator as accurately as possible.

(iii) Re-design a controller for the single degree of freedom ALPS control system to achieve the highest stiffness as possible. {Highest stiffness will have the lowest motion in response to external forces}

C. Summary

In this design, we first analyzed the assumed model of the single degree ASPS bearing actuator, and obtained the plant dynamics equations. By linearizing the plant dynamics equations, we designed the cascade and feedback compensators such that a stable and satisfied result was obtained. The specified feedback compensator was computer simulated with the nonlinearized plant dynamics equations. The results indicated that an unstable output occurred. In other words, the designed feedback compensator is fail. The failure of the design is due to the Taylor's series expansion does not converge.

II. Modelling of the single degree ASPS bearing actuator

A. Assumptions of the model

The single degree ASPS bearing actuator consists of two pairs of magnetic coil elements, mounted in opposition, to control the rim (suspended mass) along a single axis. Figure 4 shows the configuration of the actuator. The magnetic coil elements have current biasing superimposed by a controlled DC voltage source to produce a force to suspend and point the rim. For fine pointing application, the gap distances between the rim and actuators are kept to a predetermined value(<0.3").

figure 4.

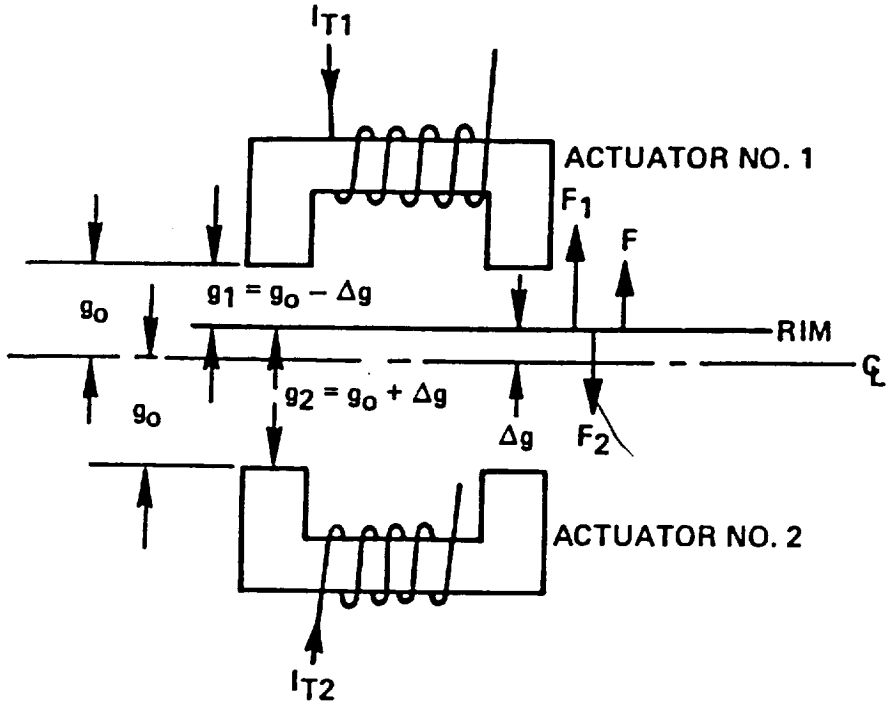

We derived the equation for the single ALPS bearing actuator with the following assumptions:

(i) The force of attraction between magnetized bodies is given by $F = (1/2u) * B^2 * \text{area}$.

(ii) The magnetic flux density is uniform between the gap, or gap distance << size of actuator.

(iii) The rim is a perfect conductor. That is, it does not support any magnetic field strength (H) inside the rim.

(iv) There is no coupling effect between each coil elements.

(v) The controlled electromagnet behaves linearly, and there is no loss or fringing of magnetic field.

(vi) The rim has a plane area over the magnetic coil assemblies.

B. Derivation of ASPS Dynamics

a) B-field in the air-gap.

From magnetic circuit theory, the total current linked by the path of an N-turn coil is given by

$$\sum_i H_i l_i = N i \qquad (4)$$

Assume

(i) the magnetic material is approximated by $B_m = \mu_m H_m + B_o$ where B_o is a constant.

(ii) gap distant at path (1) = gap distance at path (2)

ie. $g_1 = g_2 = g$

(iii) from boundary condition, B inside the coil ≈ B in

the gap.

Therefore, equation (1) becomes,

$$H_1 g_1 + H_2 g_2 + H_m l = Ni$$

$$\rightarrow 2Hg + \frac{B_m - B_o}{\mu_m} l = Ni \quad \text{(because the rim is a perfect conductor)}$$

$$\rightarrow 2Hg + \frac{\mu_o}{\mu_m} lH = Ni + \frac{B_o l}{\mu_m}$$

As the term $B_o(l/\mu_m)$ can be equivalently assigned to a magnetomotive force (mmf) $(B_o/\mu_m)l = NI_o$

So

$$2Hg + \frac{\mu_o l}{\mu_m} H = Ni + NI_o$$

Thus the magnetic flux density at the gap is given by

$$B = \mu_o H = \frac{\mu_N (i + I_o)}{2g + \frac{\mu_o}{\mu_m} l}$$

As for the particular material we used for actuator, $\mu_m >> \mu_o$. Hence

$$B \approx \frac{\mu_o N (i + I_o)}{2g} \qquad (2)$$

b) Relationship between F, I and g

By considering the stored magnetic energy, Bohr[5] and Hayt[6] were able to relate the magnetic attraction force to the magnetic flux density and cross-sectional,

$$F_m = \frac{1}{2\mu_o} B^2 * area$$

The geometry we used is similar to Humphris[7] and Groom[8], figure 4, which have two electromagnets positioned opposite the rim. This kind of configuration is more linear if we separate the magnetic flux density into the controlled and bias components.[7]

Assume no coupling effect between the two actuators, by equation (2):

$$B_1 = \frac{\mu_o N_1 (i_1 + I_1)}{2g_1}; \quad B_2 = \frac{\mu_o N_2 (i_2 + I_2)}{2g_2}$$

Let $N_1 = N_2 = N$, $I_1 = I_2 = I_o$, $i_1 = -i_2 = i$ = controlled current. Therefore, the total force acting on the rim is given by

$$F = F_1 - F_2 = \frac{(2A)}{2\mu_o}(B_1^2 - B_2^2) = \frac{A}{\mu_o}(B_1 + B_2)(B_1 - B_2)$$

$$\textit{Consider}\quad B_1 - B_2 = \frac{\mu_o N}{2}\left[\frac{I_o + i}{g_o - x} - \frac{I_o - i}{g_o + x}\right]$$

$$= \frac{\mu_o N}{2}\left[\frac{(g_o + x)(I_o + i) - (g_o - x)(I_o - i)}{g_o^2 - x^2}\right]$$

$$= \frac{\mu_o N}{2(g_o^2 - x^2)}\left[g_o(I_o + i - I_o + i) + x(I_o + i + I_o - i)\right]$$

$$= \frac{\mu_o N}{2(g_o^2 - x^2)}(2g_o i + 2I_o x) = \frac{\mu_o N(g_o i + I_o x)}{g_o^2 - x^2}$$

$$\textit{Similiarly,}\quad B_1 + B_2 = \frac{\mu_o N}{2}\left[\frac{I_o + i}{g_o - x} + \frac{I_o - i}{g_o + x}\right] = \frac{\mu_o N}{g_o^2 - x^2}(g_o I_o + xi)$$

$$\textit{Thus}\quad F = \frac{A}{\mu_o}(B_1 + B_2)(B_1 - B_2) = \frac{A}{\mu_o}\left[\frac{\mu_o N(g_o i + I_o x)}{g_o^2 - x^2}\right]\left[\frac{\mu_o N(g_o I_o + xi)}{g_o^2 - x^2}\right.$$

$$= \frac{\mu_o N^2 A(g_o i + I_o x)(g_o I_o + xi)}{(g_o^2 - x^2)^2}$$

By the Taylor's Series Expansion at the equilibrium point (x_o, i_o), we get

$$F(x,i) \approx F(x_o,\ i_o) + (x - x_o,\ i - i_o) * \nabla F|_{(x_o,\ i_o)}$$

$$as\ \frac{\partial F}{\partial i} = \frac{\mu_o N^2 A}{(g_o^2 - x^2)^2}\left[g_o(g_o I_o + xi) + x(g_o i + I_o x)\right]$$

$$\frac{\partial F}{\partial x} = \frac{\mu_o N^2 A}{(g_o^2 - x^2)^4}\left[(g_o^2 - x^2)^2\left[I_o(g_o I_o + xi) + i(g_o i + I_o x)\right]\right.$$

$$\left. - 2(g_o^2 - x^2)(-2x)(g_o I_o + xi)(g_o i + I_o x)\right]$$

at equilibrium point $(x_o,\ i_o) = (0,\ 0)$,

$$F(x_o,\ i_o) = 0$$

$$\frac{\partial F}{\partial x}|_{(x_o,\ i_o)} = \frac{\mu_o N^2 A I_o^2}{g_o^3}$$

$$\frac{\partial F}{\partial i}|_{(x_o,\ i_o)} = \frac{\mu_o N^2 A I_o}{g_o^2}$$

So

$$F(x,\ i) \approx x * \frac{\partial F}{\partial x}|_{(x_o,\ i_o)} + i * \frac{\partial F}{\partial i}|_{(x_o,\ i_o)}$$

$$= \left(\frac{\mu_o N^2 A I_o^2}{g_o^3}\right) x + \left(\frac{\mu_o N^2 A I_o}{g_o^2}\right) i \qquad (3)$$

c) V-I relationship of the actuator.

Recall equation (2):

$$B = \frac{\mu_o N(i + I_o)}{2g}$$

By definition, $\Phi=NBA$ and $L=(d\Phi/di)$[5]. Therefore, the inductance of the gap is

$$L_1 = NA\frac{dB}{di} = \frac{N^2A\mu_o}{2g} \tag{4}$$

and the inductance of the whole circuit is

$$L = L_1 + L_2 + L_c =$$

$$= \frac{N^2A\mu_o}{2g_1} + \frac{N^2A\mu_o}{2g_2} + L_c \qquad \text{(by 4)}$$

$$= \frac{N^2A\mu_o g_o}{g_o^2 - x^2} + L_c$$

By Kirchhoff's voltage law, we have

$$V = Ri + \frac{d}{dt}(Li)$$

$$= Ri + L\frac{di}{dt} + i\frac{dl}{dx} * \frac{dx}{dt}$$

We previously separated the voltage, current and gap distance into the bias components and controlled components.

That is Let $V = V_b + v$

$$i = I_b + i$$

and $x = g_o + x$

Therefore,

$$V_b + v = R(I_b + i) + L\frac{di}{dt} + i\frac{dl}{dx}*\frac{dx}{dt} + I_b\frac{dl}{dx}*\frac{dx}{dt}$$

As, at equilibrium position, $V_b = RI_b$, assume $i \approx 0$, $x \approx 0$

Therefore,

$$i\frac{dL}{dx}*\frac{dx}{dt} \approx 0$$

$$so \quad v = Ri + L\frac{di}{dt} + I_b\frac{dL}{dx}*\frac{dx}{dt}$$

$$Consider \quad \frac{dL}{dx} = \frac{2N^2A\mu_o g_o}{g_o^2 - x^2}x$$

$$\therefore \quad I_b*\frac{dL}{dx}*\frac{dx}{dt} = I_b\frac{2N^2A\mu_o g_o}{(g_o^2 - x^2)^2}*x*\frac{dx}{dt} \approx 0$$

$$Thus \quad v(t) = Ri(t) + L\frac{d}{dt}i(t)$$

taking the Laplace transform on both sides, we get

$$V(s) = RI(s) + LsI(s)$$

$$or \; I(s) = \frac{1}{R + Ls}V(s) \qquad (5)$$

Recall equation (3)

$$F(x,\ i) = \frac{A\mu_o N^2 I_o^2}{g_o^3}x + \frac{A\mu_o N^2 I_o}{g_o^2}i$$

$$By\ Newton\ Second\ Law\ \ F(x,\ i) = m\frac{d^2x}{dt^2}$$

$$So,\ \ m\frac{d^2x}{dt^2} = \frac{A\mu_o N^2 I_o^2}{g_o^3}x + \frac{A\mu_o N^2 I_o}{g_o^2}i$$

Taking the Laplace Transform on both sides, we get

$$ms^2\mathbf{X}(s) = \frac{A\mu_o N^2 I_o^2}{g_o^3}\mathbf{X}(s) + \frac{A\mu_o N^2 I_o}{g_o^2} * \frac{1}{R + Ls}V(s)$$

$$or\ \frac{\mathbf{X}(s)}{V(s)} = \frac{\dfrac{A\mu_o N^2 I_o}{g_o^2}}{(R + Ls)\left(ms^2 - \dfrac{A\mu_o N^2 I_o^2}{g_o^3}\right)} \qquad (6)$$

$$= \frac{\dfrac{A\mu_o N^2 I_o}{g_o^2 mL}}{\left(s + \dfrac{R}{L}\right)\left(s^2 - \dfrac{A\mu_o N^2 I_o^2}{m\ g_o^3}\right)}$$

$$Let\ a = \frac{A\mu_o N^2 I_o}{g_o^2 mL},\quad b = \frac{R}{L},\quad c^2 = \frac{A\mu_o N^2 I_o^2}{m\ g_o^3}$$

Therefore the plant dynamics of the ALPS actuator are

$$G_p(s) \triangleq \frac{\mathbf{X}(s)}{V(s)} = \frac{a}{(s + b)(s^2 - c^2)}$$

Which is similar to the plant dynamic equation obtained by

Kilgore[9] and Jayawant[3].

Referring to Groom[2], the values of those parameters are,

I_o	0.57 Amps
A	$1.1400918*10^{-3}$ m^2
μ_o	$4 \pi *10^{-7}$ H m^{-1}
N	1386 turns per coil
m	7.19712 kg
g_o	0.00762 m
R	8.0 Ω
L	0.1805899 h at g_o

$$\therefore \quad a \approx 20.79$$

$$b = 44.3$$

$$c^2 \approx 280.8$$

Thus, the open loop transfer function is

$$G_p = \frac{20.79}{s^3 + 44.3s^2 - 280.8s - 12439.59}$$

d) Discussion of the plant dynamic of ASPS actuator

The open loop transfer function is a third order, type zero, all poles plant system. The characteristic equation also contains one positive real root, so this plant is not BIBO stable. The pole zero diagram of the plant is shown in fig 5. In order to move the open loop unstable root into the stable region, we need to add zeros in the left half plane so that the locus are pulled into the stable region. In other word, a reshaping of the root locus (compensator) is necessary.

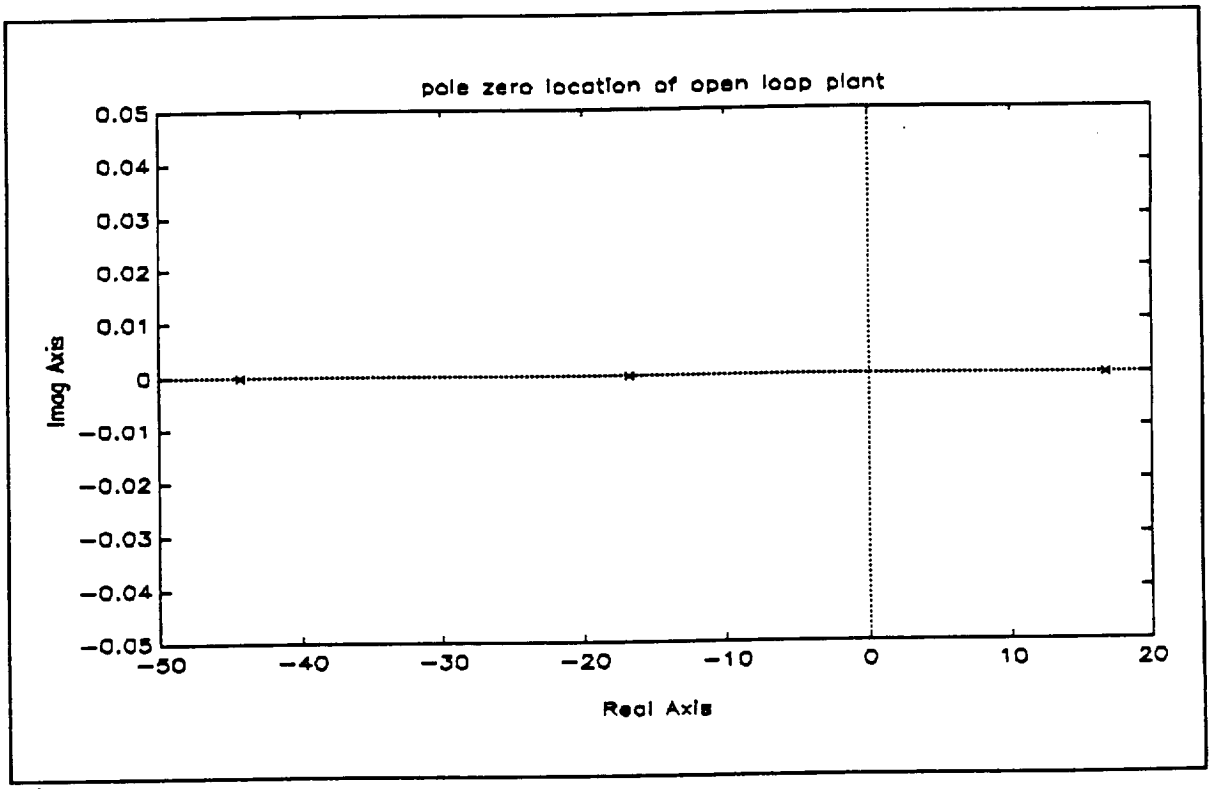

figure 5

III. Compensators Design

A. Cascade Compensator

The approach we used in the cascade compensator is to achieve the goal (shift the root locus to the L.H.P.) with minimum complexity. For the simplest case, by the knowledge that a pole will pull the root locus to the right, a zero will pull the root locus to the left and a pole-zero pair close to the origin will decrease the steady state step error (G_p is type zero), we tried the general lag-lead cascade compensator[10],

$$G_c(s) = A \frac{(s + \frac{1}{T_1})}{(s + \frac{1}{\alpha T_1})} \quad \frac{(s + \frac{1}{T_2})}{(s + \frac{\alpha}{T_2})}$$

with α =10, and gain A. [10] The lag component was fixed at

(s+ 0.05)/(s+ 0.005) and the lead component was moved along the real axis. Some root locus results are shown in appendix I. After studying the results, we decided that we needed to increase the compensator complexity in order to meet the design specifications.

Since the lag component only affected the steady state error, for simplicity, we tried the dual phase advanced compensator with α=10.

$$G_c(s) = \left(\frac{s + \frac{1}{T}}{s + \frac{\alpha}{T}}\right)^2$$

Some root locus results were shown in the appendix II.

Interestingly, when we put the double zero near to the second large negative real pole of the open-loop transfer function, a significant portion of the root locus were pulled into the left half plane, figure 6. This was the result we were looking for.

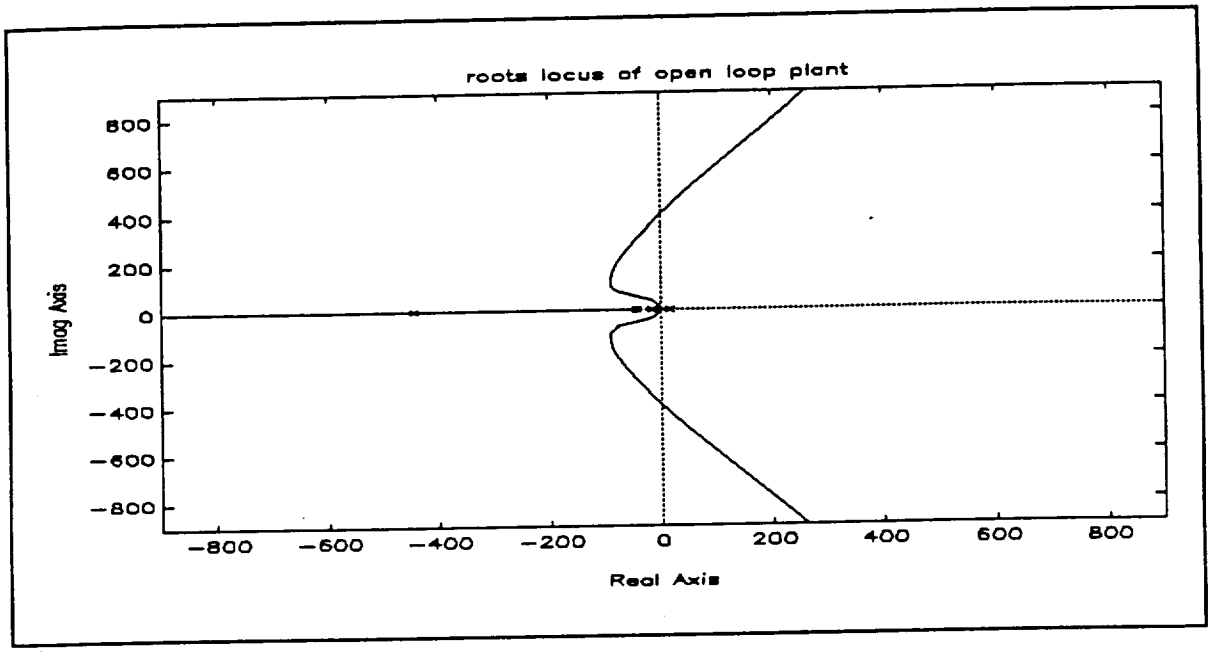

figure 6

Addition of a lag component in the compensator only reduced the steady state step error slightly (0.02), so for simplicity, we used the dual phase advanced compensator

$$G_c(s) = \left(\frac{s + 44.3}{s + 443}\right)^2$$

A block diagram is shown in figure 7. We selected a damping ratio $\xi = 0.7$, and the maximum natural frequency. The figures of merit are,

poles: -86.15 ± 87.89j, -93.24, -620.46

additional gain K = 1.011406 E 6

steady state step error = 0.06

rise time = 0.009 sec.

peak overshoot = 1.42

peak time = 0.025 sec.

settling time = 0.05 sec. (for 5%)

gain margin = 16.75 dB

phase margin = 180°

stiffness, ω_n = 15 kN $kg^{-1}m^{-1}$

stability region : 6.0939 E 4 < K < 6.8041 E 6

The step response was shown in figure 8, and the Bode plot was shown in figure 9. Those results are obtained by matlab.

figure 7.

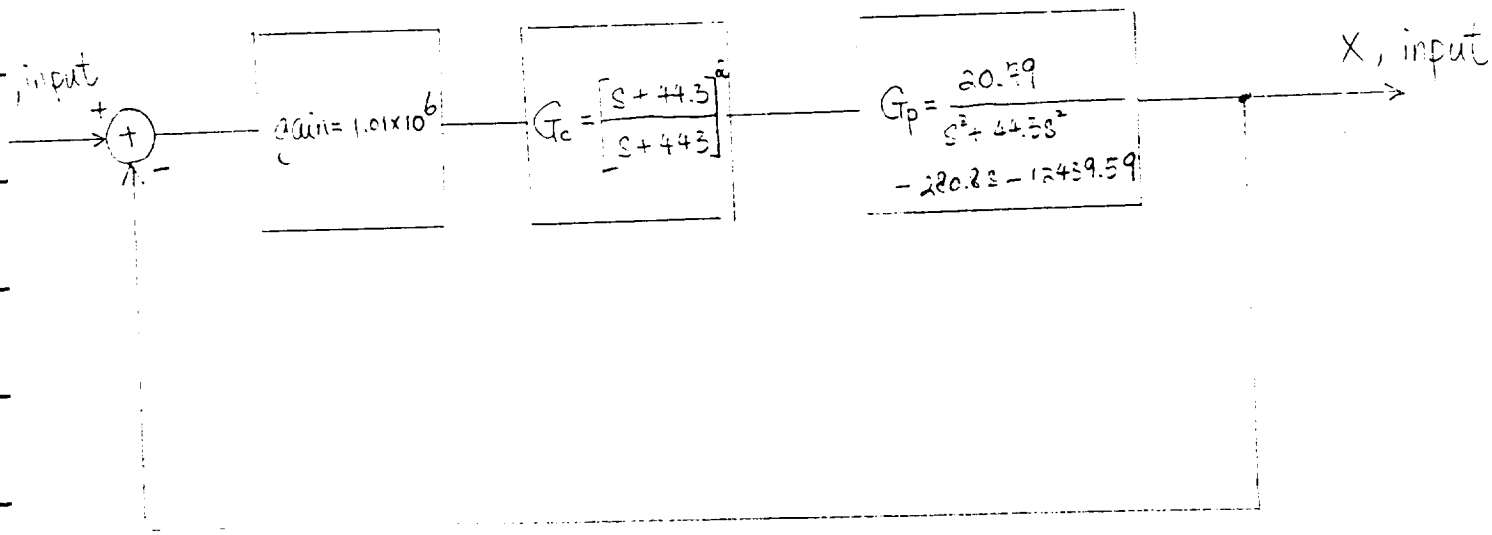

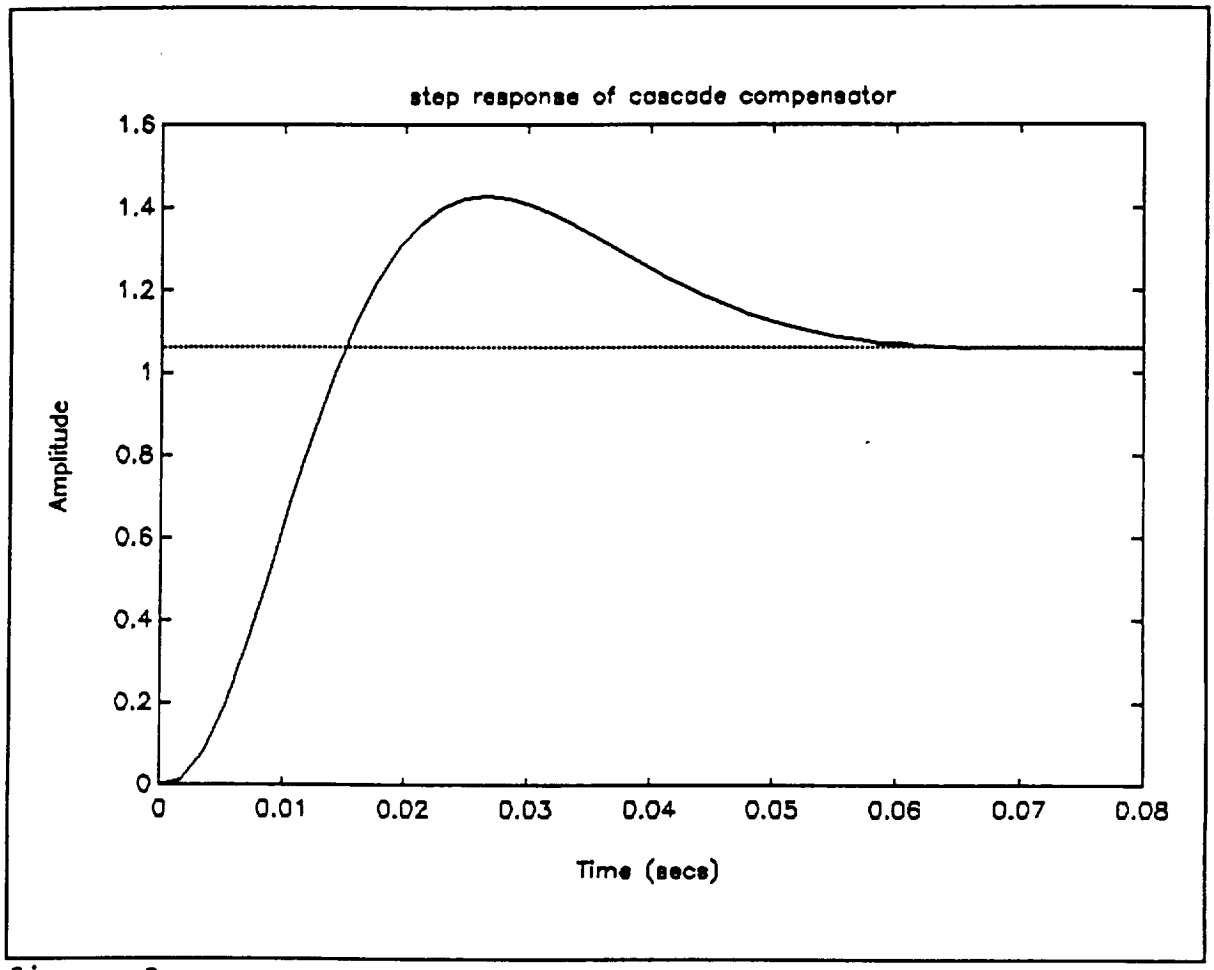
step response of cascade compensator
Amplitude
Time (secs)
1.6
1.4
1.2
1
0.8
0.6
0.4
0.2
0
0
0.01
0.02
0.03
0.04
0.05
0.06
0.07
0.08

figure 8

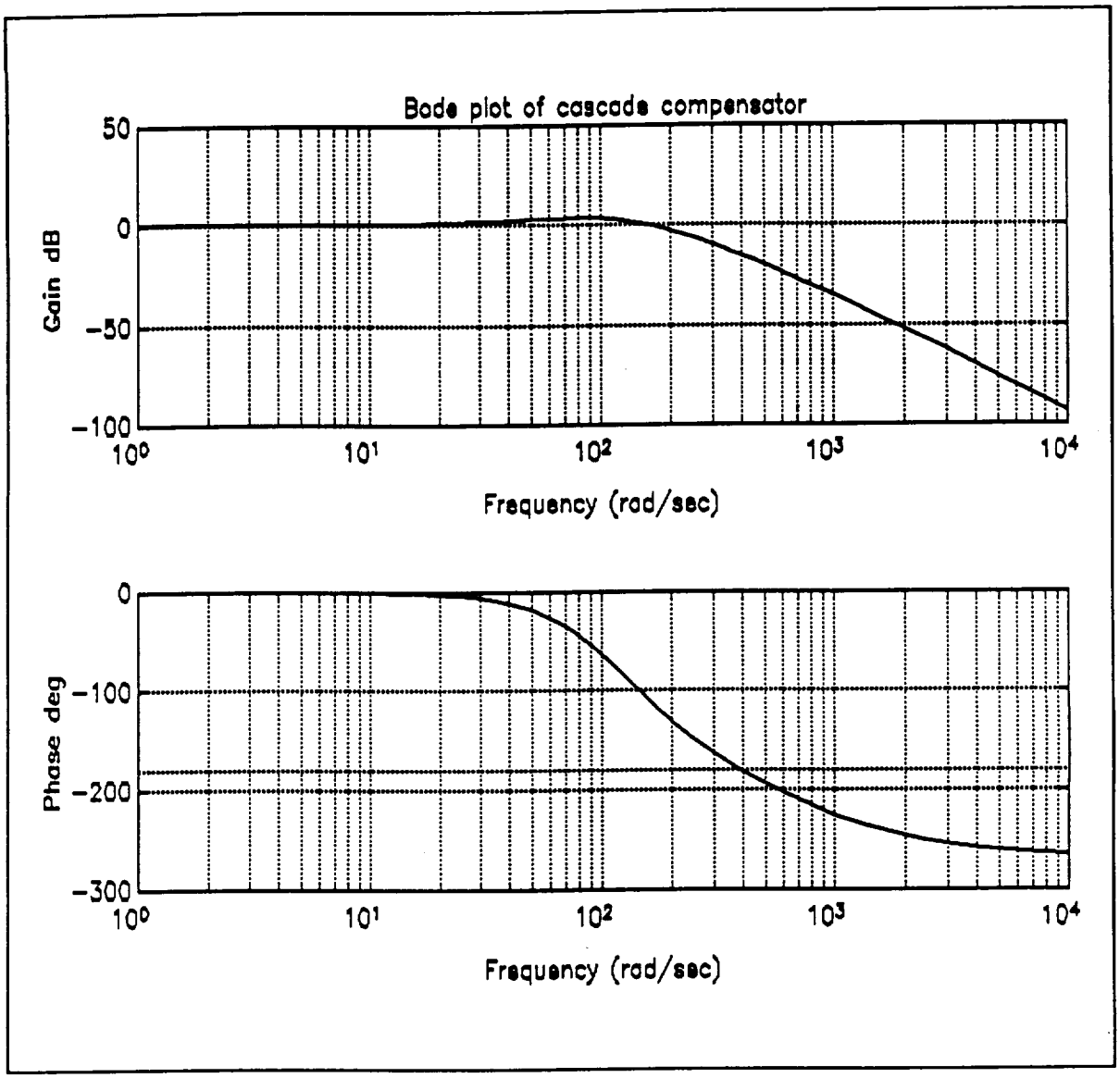
Bode plot of cascade compensator
50
0
−50
−100
Gain dB
10^0
10^1
10^2
10^3
10^4
Frequency (rad/sec)
0
−100
−200
−300
Phase deg
10^0
10^1
10^2
10^3
10^4
Frequency (rad/sec)

figure 9

B. Feedback Compensator Design

The cascade compensator will be converted to a digital controller later, and a computer will be involved to control the plant. Therefore, it is natural to design the compensator using the state feedback technique. This technique is flexible and convenient to implement. A brief derivation of the design procedure is shown in Appendix III. In the case where some state variables are not accessible, an observer (estimator) may be used. Observer design procedures are also shown in the Appendix III. This material are come D'Azzo [10]. In this design, we used the full state feedback technique.

A state space representation of the open loop plant is shown in the figure 10.

figure 10

State space representation of the open loop plant

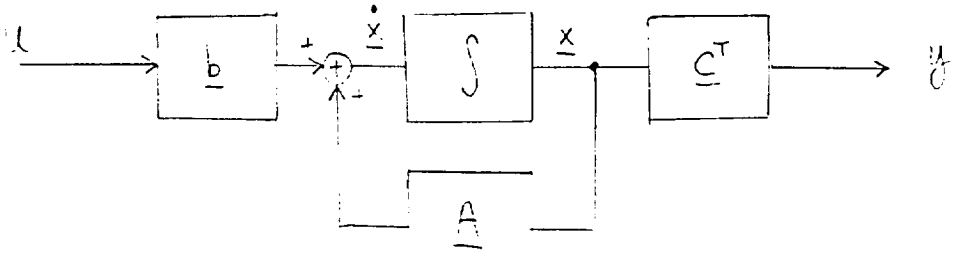

$$\frac{d}{dt}\begin{bmatrix} x_1 \\ x_2 \\ x_3 \end{bmatrix} = \begin{bmatrix} 0 & 1 & 0 \\ 0 & 0 & 1 \\ -44.3 & 280.8 & 12439.59 \end{bmatrix}\begin{bmatrix} x_1 \\ x_2 \\ x_3 \end{bmatrix} + \begin{bmatrix} 0 \\ 0 \\ 20.79 \end{bmatrix} u$$

$$y = \begin{bmatrix} 1 & 0 & 0 \end{bmatrix}\begin{bmatrix} x_1 \\ x_2 \\ x_3 \end{bmatrix}$$

The controllability matrix is,

$M_C=[b|Ab|A^2b]$

=

$$\left|\begin{array}{c|c|c} 0 & 0 & 20.79 \\ 0 & 20.79 & -920.997 \\ 20.79 & -920.997 & 46637.99 \end{array}\right|$$

as $\det(M_C) \neq 0$, so M_C has full rank.

The observability matrix is

$M_O=[C^T|A^TC^T|(A^T)^2C^T]$

=

$$\left|\begin{array}{c|c|c} 1 & 0 & 0 \\ 0 & 1 & 0 \\ 0 & 0 & 1 \end{array}\right|$$

So M_O has full rank. Hence, this system is completely controllable and completely observable.

Motivated by the performance of the cascade compensator, we selected the poles of the control ratio to be $-86.15 \pm 87.89j$, -100, which give us a good step response. A block diagram is shown in the figure 11. The figures of merit are,

gain = 72.8546 E 3

$k_1 = 1.01$

k_2 = 0.021561

k_3 = 0.0001505

poles : -86.15 ± 87.89j, -100

steady state step error = 0

rise time = 0.03 sec.

settling time = 0.045 sec. (for 5 %)

gain margin = 13 dB

phase margin = 160°

stiffness = 15 $kNkg^{-1}$ m^{-1}

A step response and Bode plot were shown in figure 12 and figure 13 respectivity. Those results are obtained by matlab.

figure 11.

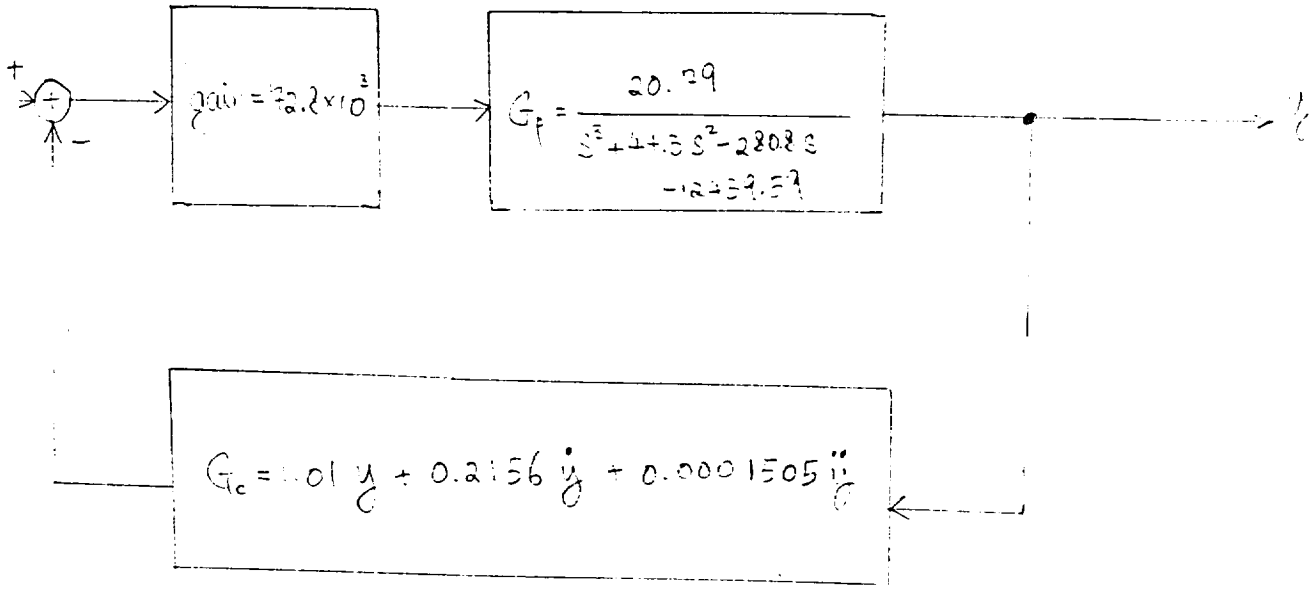

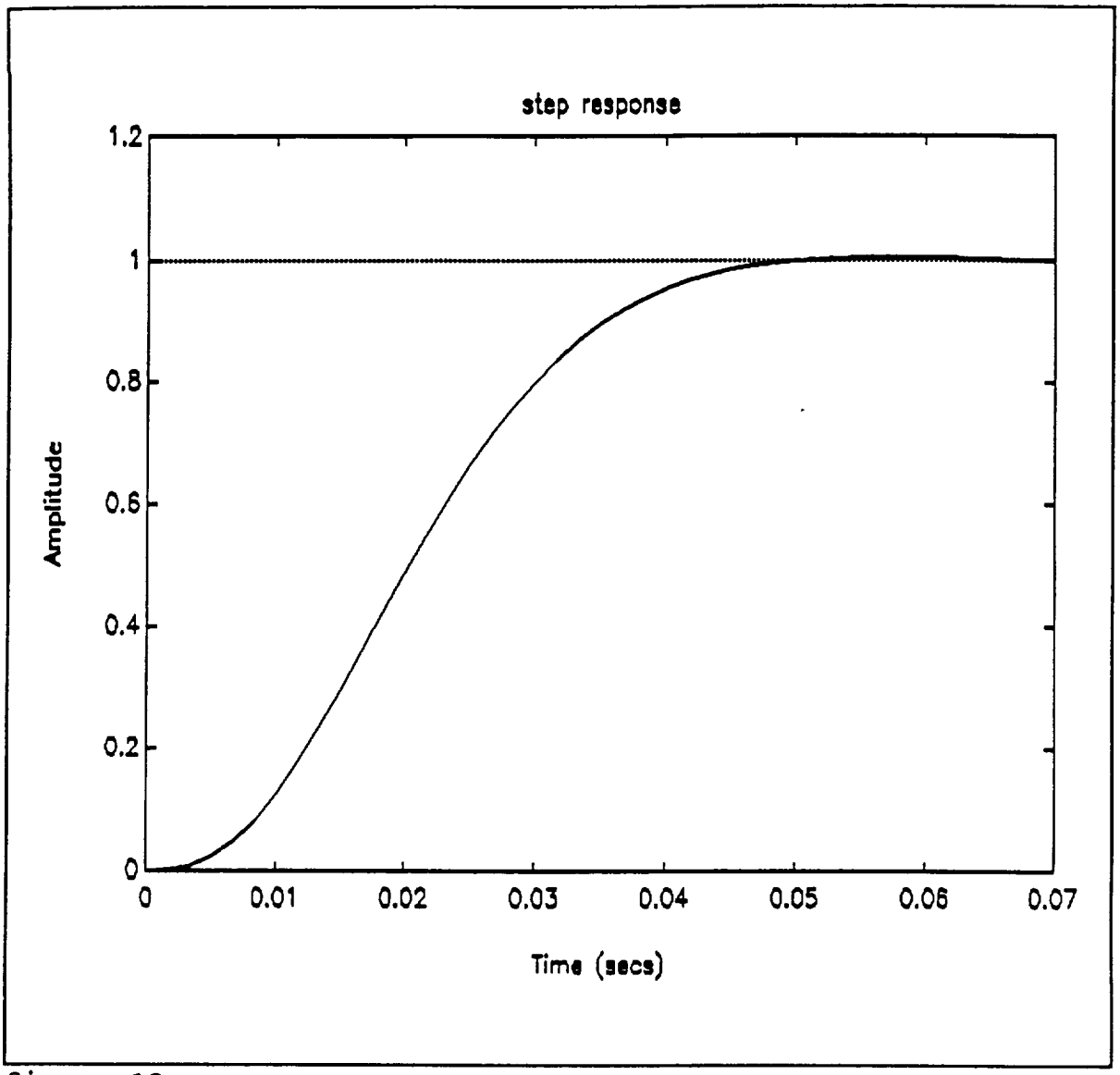
step response
1.2
1
0.8
0.6
0.4
0.2
0
Amplitude
0
0.01
0.02
0.03
0.04
0.05
0.06
0.07
Time (secs)

figure 12

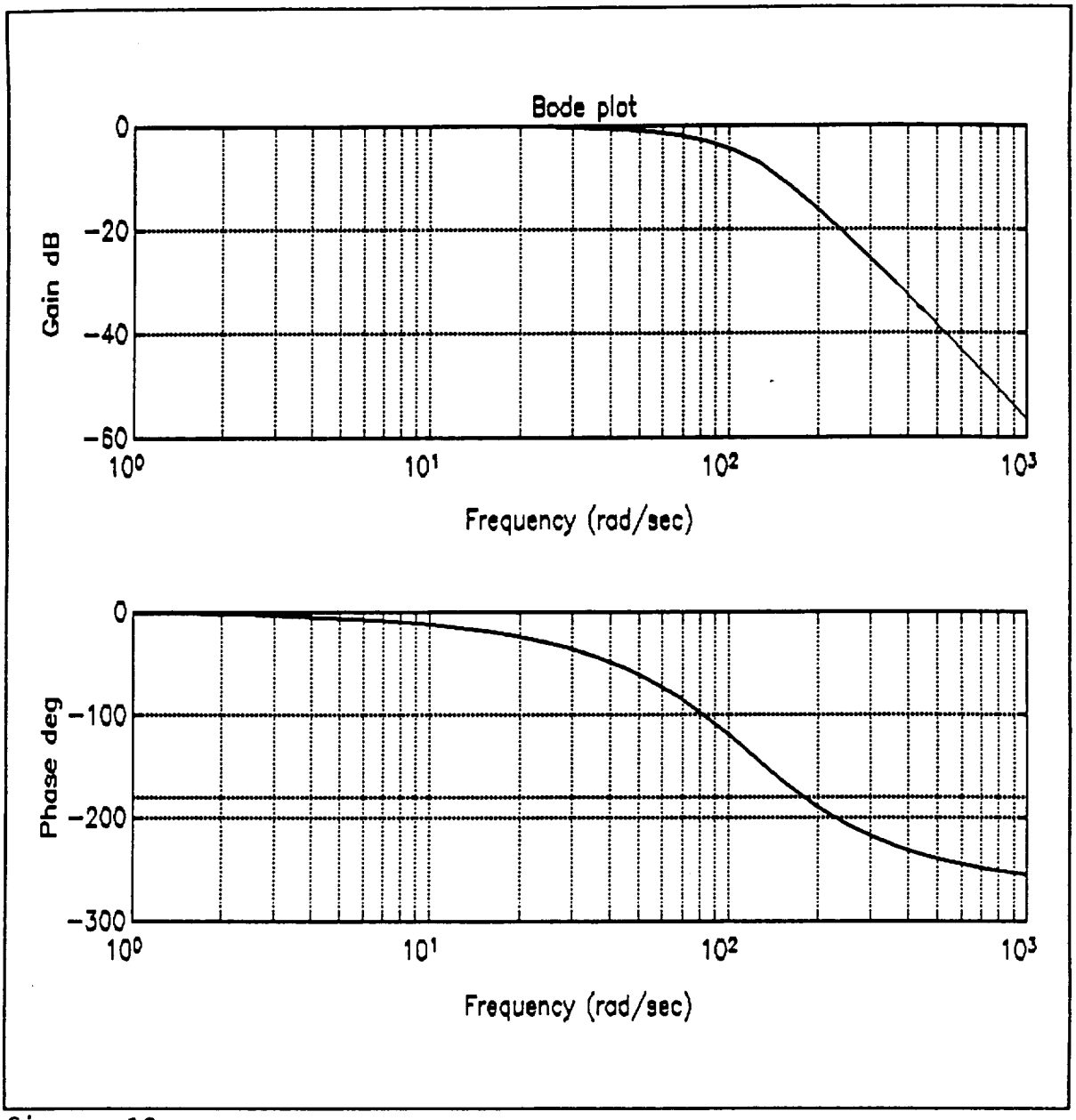
Bode plot
0
-20
-40
-60
Gain dB
10^0
10^1
10^2
10^3
Frequency (rad/sec)
0
-100
-200
-300
Phase deg
10^0
10^1
10^2
10^3
Frequency (rad/sec)

figure 13

IV Computer Simulation

We simulated the state feedback design by a four order Runge Kntta Method in the time domain. The Runge Kntta Method is a special version of the general Taylor's series expansion.

For a general different equation,

$$\frac{d\vec{X}}{dt} = \vec{f}(\vec{X})$$

Let,

$$\vec{f}_1 = \vec{f}(\vec{X})$$

$$\vec{f}_2 = \vec{f}(\vec{X} + \frac{1}{2} h \vec{f}_1)$$

$$\vec{f}_3 = \vec{f}(\vec{X} + \frac{1}{2} h \vec{f}_2)$$

$$\vec{f}_4 = \vec{f}(\vec{X} + h \vec{f}_3)$$

The next $\vec{X}$ can be approximated by

$$\vec{X}_{next} = \vec{X} + \frac{h}{6} [\vec{f}_1 + 2(\vec{f}_2 + \vec{f}_3) + \vec{f}_4]$$

with an error of fifth power term of the Taylor series expansion. The h is the increment step side.

Recall,

$$m\ddot{x} = \frac{A\mu_o N^2 (g_o I_o + x i)(g_o i + I_o x)}{(g_o^2 - x^2)^2}$$

$$v = R i + L\frac{di}{dt}$$

Let

$$x_1 = x = \text{output}$$

$$x_2 = \frac{dx_1}{dt}$$

$$x_3 = i$$

$$x_4 = t$$

$$v = u = \text{input}$$

So

$$\dot{x}_1 = x_2$$

$$\dot{x}_2 = \dot{x} = \frac{\frac{A\mu_o N^2}{m} (g_o I_o + x_1 x_3)(g_o x_3 + I_o x_1)}{(g_o^2 - x_1^2)^2}$$

$$\dot{x}_3 = -\frac{R}{L} x_3 + \frac{1}{L} u$$

$$\dot{x}_4 = 1$$

Let the control law be

$$u = r - (k_1 x_1 + k_2 x_2 + k_3 \dot{x}_2)$$

where r is the reference input.

In the computer code, we need to estimate the second derivative of x, which is achieved by

$$(x_{2\,present} - x_{2\,previous}) \;/\; \text{time interval}$$

For the linearized plant dynamics equations, slightly modification of the computer codes can do the job. The results of computer simulation are shown in figure 14 to 19. The computer program was written in Pascal language, and is shown in Appendix IV.

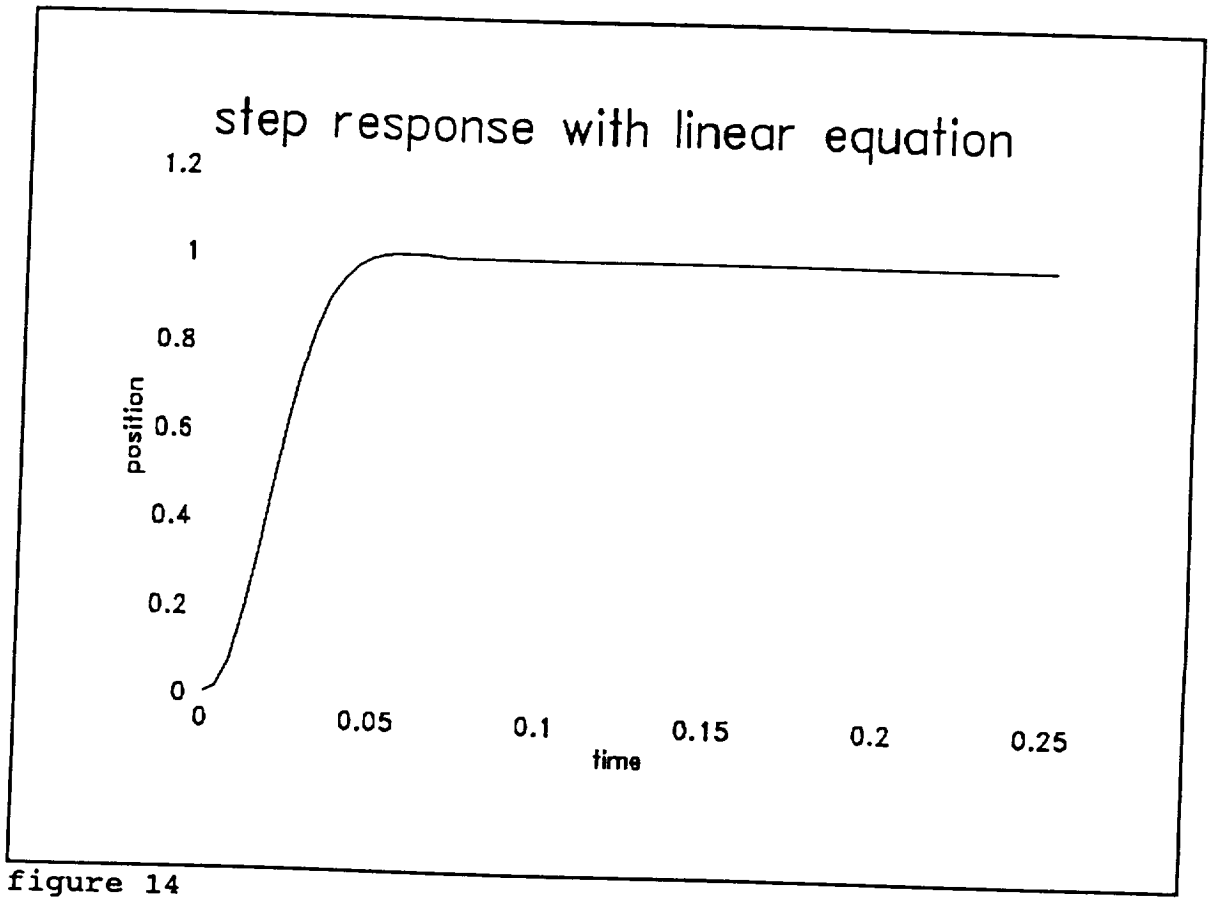

figure 14

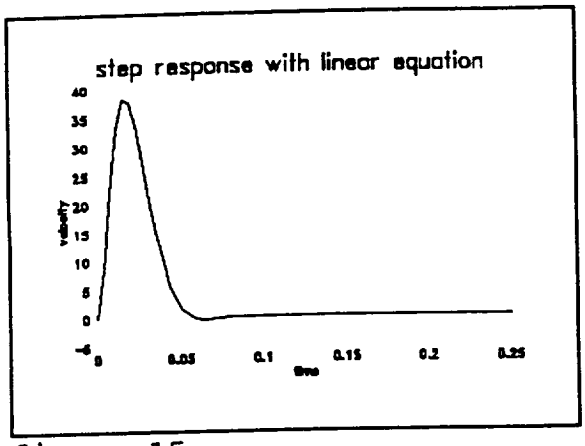

figure 15

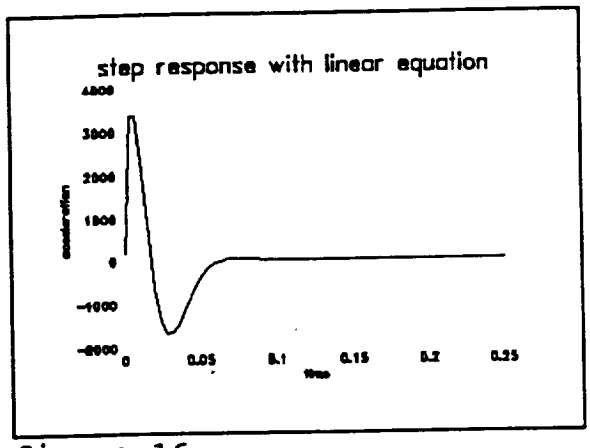

figure 16

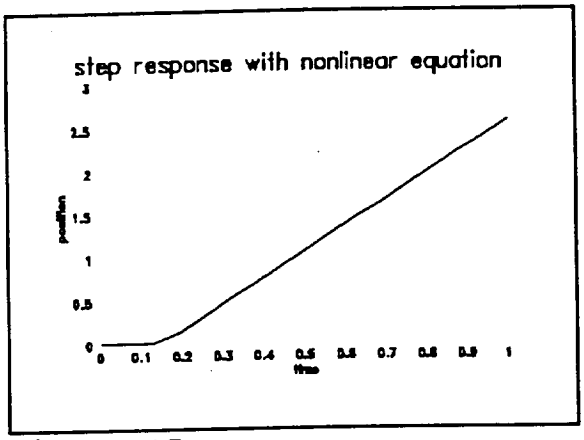

figure 17

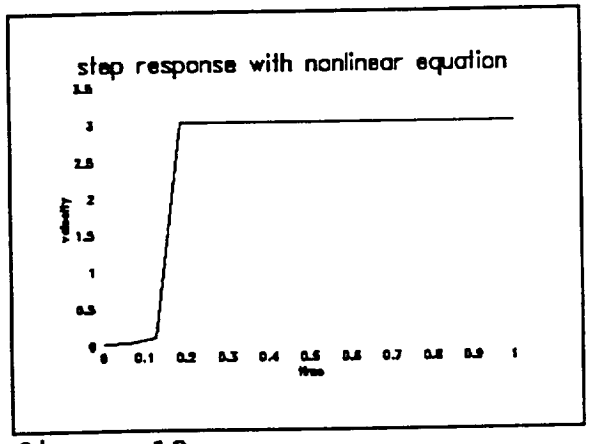

figure 18

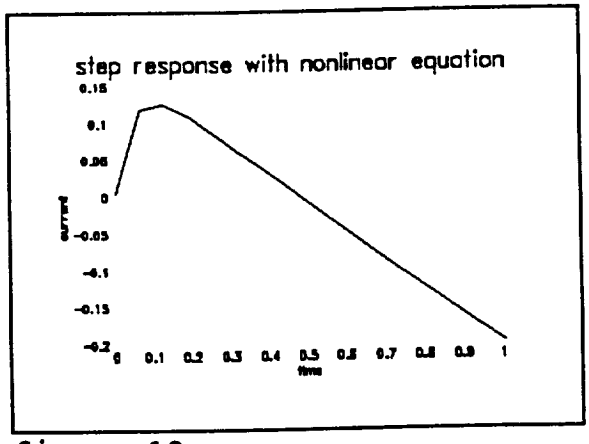

figure 19

V. Discussion of results

The computer simulation showed that the step response increased linearly with time, figure 17. That is, an unstable response occurred.

Consider the plant dynamics equations, recall

$$\ddot{x} = \frac{A\,\mu_o\,N^2\,(\,g_o\,I_o + x\,i\,)\,(\,g_o\,i + I_o\,x\,)}{(\,g_o^2 - x^2)^2}$$

As for $|\,x\,| < |\,g_o\,|$

$$\frac{1}{(g_o^2 - x^2)^2} = g_o^{-4}\,\frac{1}{(\,1 - \frac{x^2}{g_o^2})^2}$$

$$= g_o^{-4}\,[\,1 + (\frac{x^2}{g_o^2}) + (\frac{x^2}{g_o^2})^2 + \ldots\,]^2$$

$$= g_o^{-4}\,[\,1 + 2(\frac{x^2}{g_o^2}) + 3(\frac{x^2}{g_o^2})^2 + \textit{higher terms}\,]$$

$$\textit{So}\ \frac{(g_o\,I_o + x\,i)\,(g_{oi} + I_o\,x)}{(g_o^2 - x^2)^2}$$

$$= g_o^{-4}\,(g_o\,I_o + x\,i)\,(g_o\,i + I_o\,x)$$

$$[\,1 + 2(\frac{x^2}{g_o^2}) + 3(\frac{x^2}{g_o^2})^2 + \textit{higher terms}\,]$$

$$= g_o^{-4}\,(g_o\,I_o^2\,x + g_o^2\,I_o\,i + g_o\,x\,i^2 + I_o\,x^2\,i)$$

$$[\,1 + 2(\frac{x^2}{g_o^2}) + 3(\frac{x^2}{g_o^2})^2 + \ldots]$$

$$= g_o^{-4}\,[(g_o\,I_o^2\,x + g_o^2\,I_o\,i)$$

$$+ (2\,\frac{I_o^2}{g_o}\,x^3 + 3\,I_o\,x^2\,i + g_o\,x\,i^2) + \textit{higher terms}\,]$$

Obviously, the coefficient magnitude of the third terms in the Taylor's series expansion is larger than the coefficient magnitude

of the first term. Thus, at least, we need to include the third terms in the compensator design. However, we cannot use the conventional linear design theory in this situation.

Even thought we include the third terms in the design, the coefficient magnitude of the x^n terms in the series expansion increase without bounded (because $g_o < 1$). So, the Taylor's series expansion does not exist.

VI. Conclusion and recommendation

The plant dynamics equations are nonlinear, and the conventional linearization does not work. We recommend to design the compensator without linearization in the time domain.

As, in general, if we close the loop,

$$\frac{d\vec{x}}{dt} = \vec{f}\ (\ \vec{x}\ ,\ u\ )$$

$$u = g\ (r\ ,\ \vec{x}\ )$$

define PI to be

$$\int_0^{\infty} t\ (x_1 - r)^2\ dt$$

and, minimizing the PI which is subjected to the constraint equation,

$$\frac{d\vec{x}}{dt} = \vec{f}\ (\ \vec{x}\ ,\ g\ (\ r\ ,\ \vec{x}\ )\ )$$

, by the Langrange multiple method. The mathematics is too difficult to carry out, and the analysis is left for interested reader only.

Bibliography

1. Jayawant, B.V. " Review Lecture of Electromagnetic Suspension and Levitation Techniques," Proc. R. Soc. Lond. A416, 245-320 (1988).

2. Groom, N.J. " ASPS Final Design Review," Sperry Corporation Flight Systems, May 1977.

3. Hamilton, B.J. " The Development of the ALPS Vernier System," NASA NAS1-15008, June 1983.

4. Woodson, H.H. and Melcher, J.R. *Electromechanical Dynamics. Part I: Discrete Systems.* John Wiley and Sons, Inc., 1968.

5. Bohr, E.V. *Introduction to Electromagnetic Fields and Waves.* Addison-Wesley Publishing Company, 1967.

6. Hayt, W.H. *Engineering Electromagnetic.* McGraw-Hill Book Company, 1981.

7. Humphris, R.R." Introduction to Magnetic Bearings," ROMAG 91, Magnetic Bearings and Dry Gas Conference and Exhibition, March, 1991.

8. Groom, N.J." Analytical Model of an Annular Momentum Control Device Laboratory Test Model Magnetic Bearing Actuator," NASA TM-80099, Aug.,1997.

9. Kilgore, W.A." Comparison of Digital Controllers used in Magnetic Suspension and Balance Systems," M.S. Thesis, Old Dominion University, Dec. 1989.

10. D'Azzo, J.J. *Linear Control Analysis and Design: Conventional and Modern*. McGraw-Hill Publishing Company, 3rd Ed., 1988.

Appendix I

Root locus result of general lead lag cascade compensator

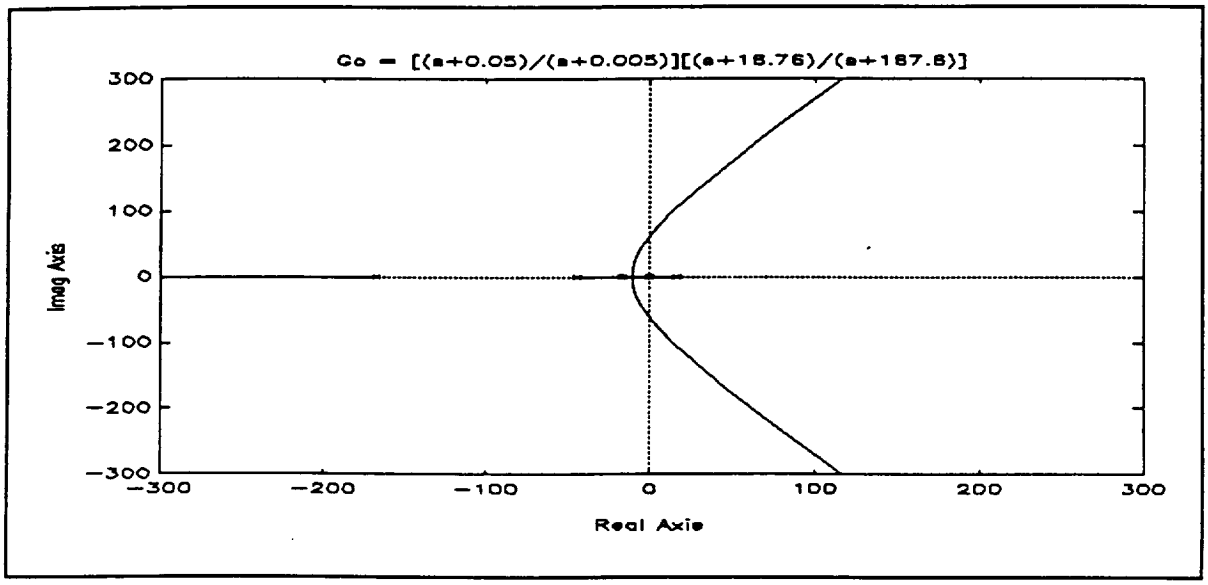

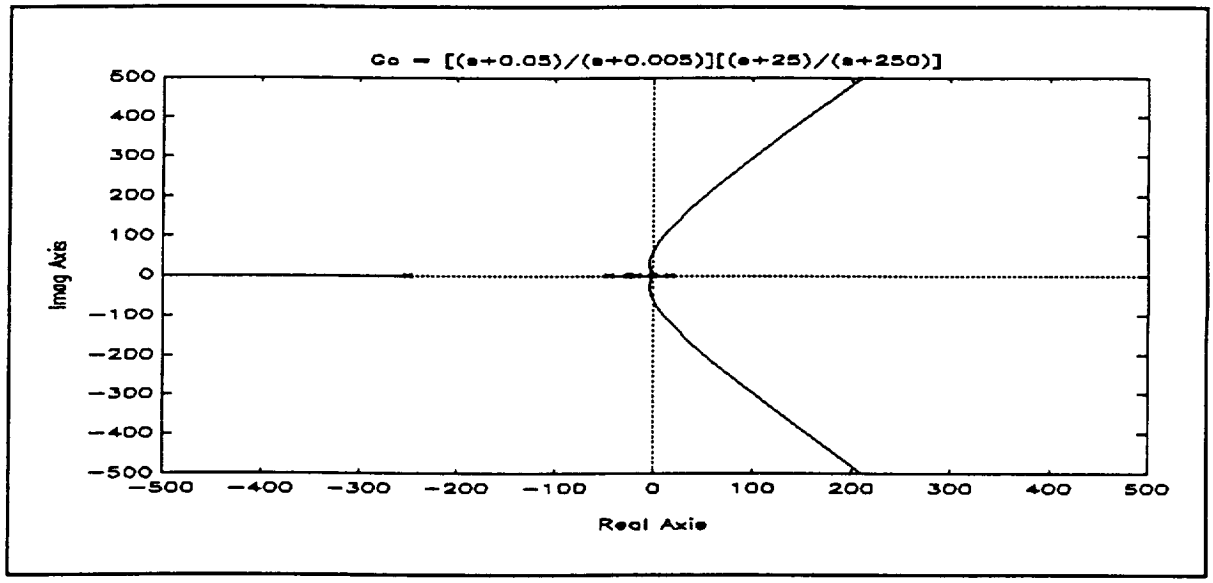

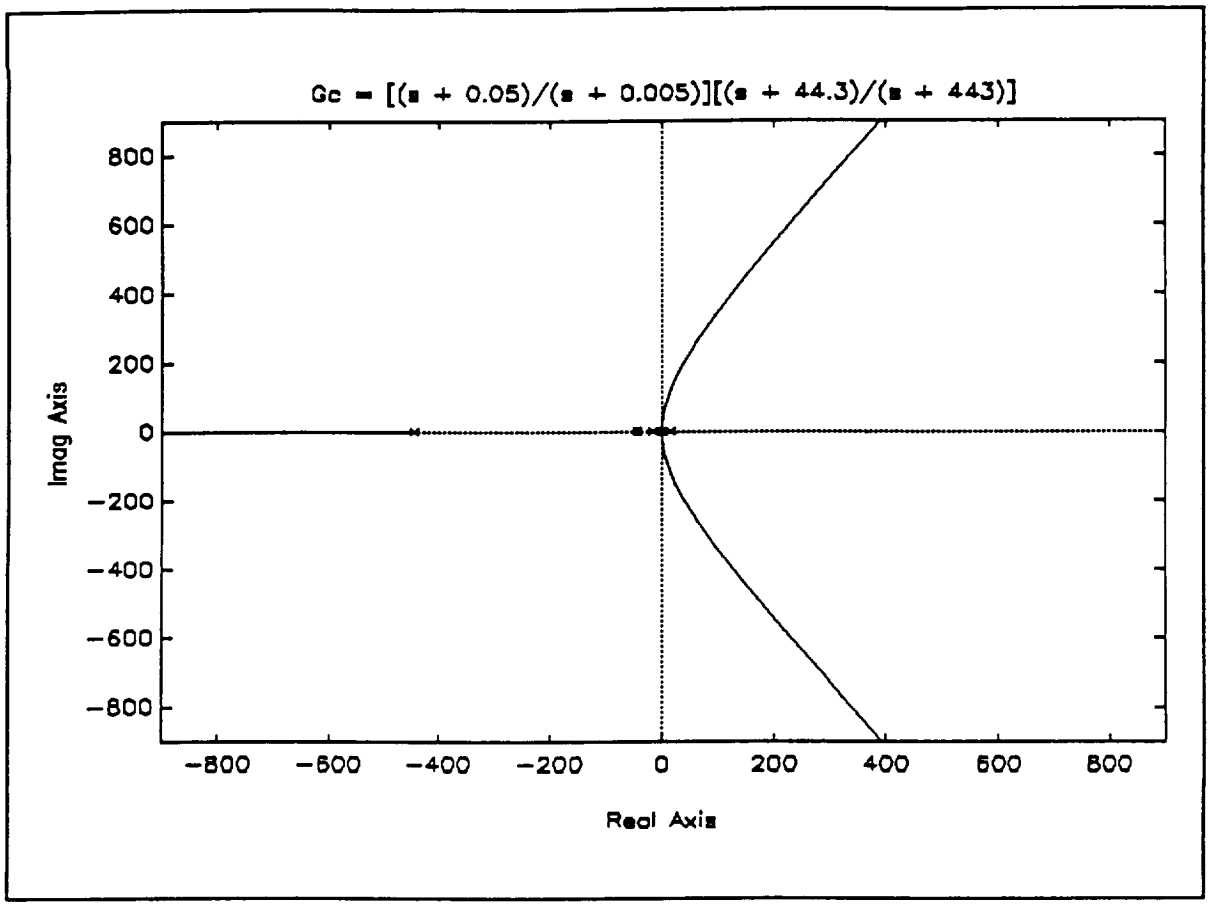

Appendix II

Root locus results of cascade dual phase advance compensator

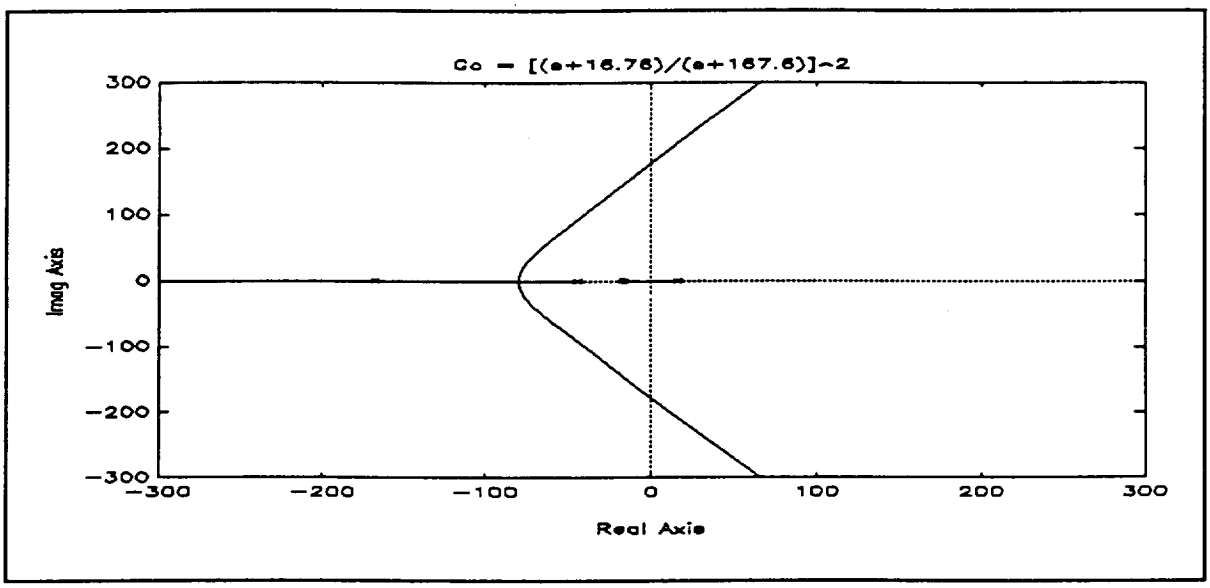

$$G_c = [(s + 44.3)/(s + 443)]^2$$

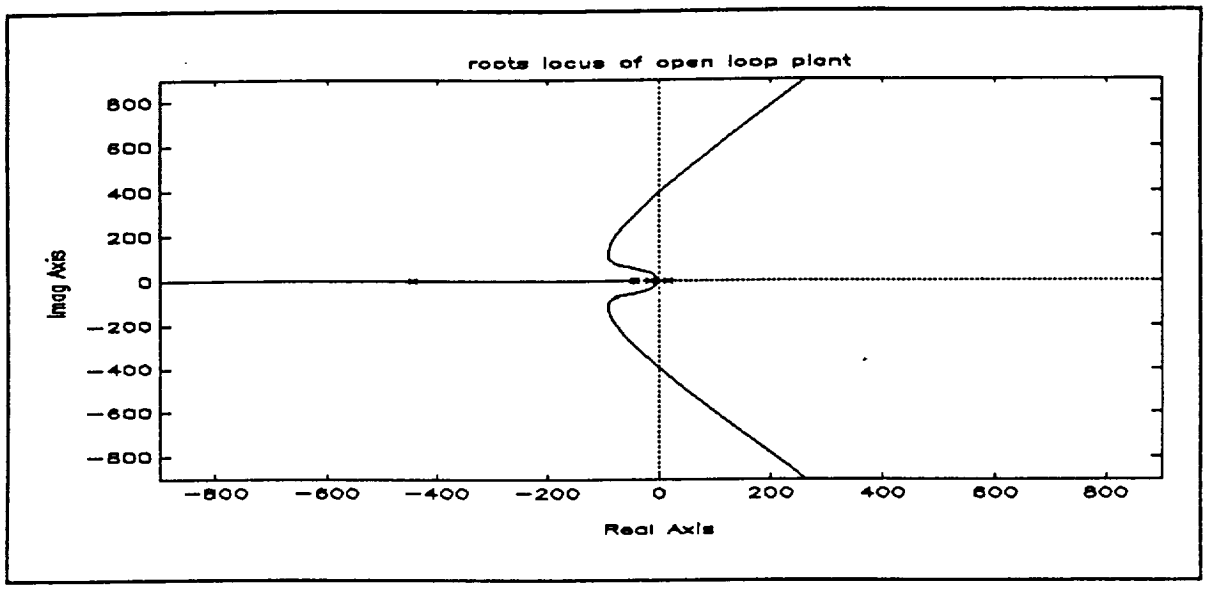

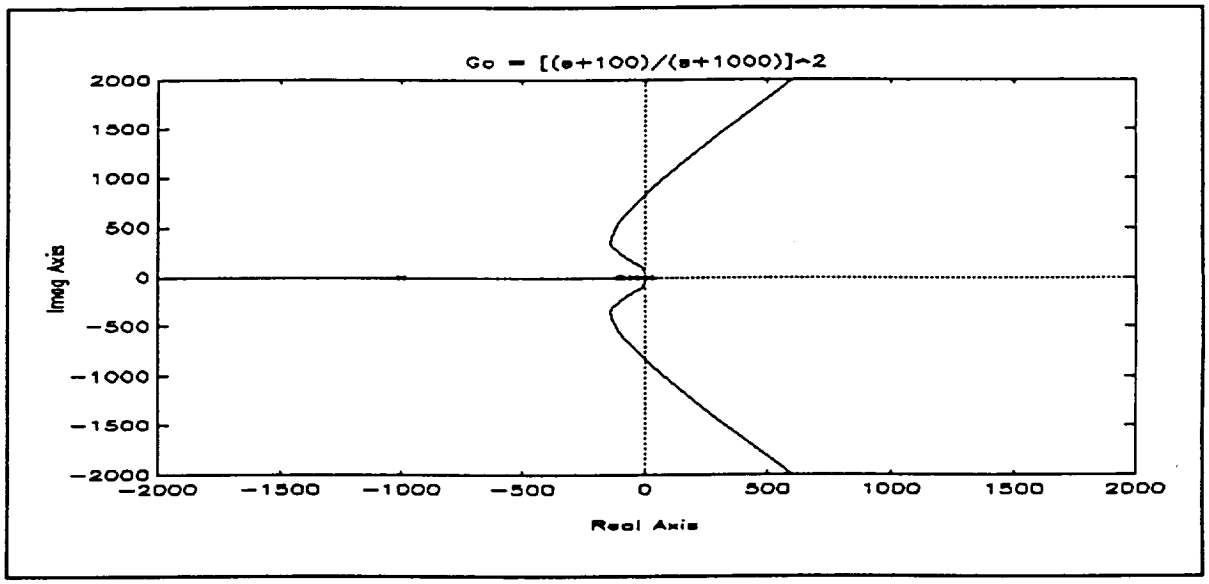

Appendix III

State feedback design procedure[10]

Let the open-loop plant transfer function be

$$G_p = \frac{c_0}{s^3 + a_2 s^2 + a_1 s + a_0} = \frac{X}{u}$$

Let, for standard notation,

$$x_1 = y, \quad x_2 = \frac{dy}{dt}, \quad x_3 = \frac{d^2y}{dt^2}$$

$$\therefore \frac{dx_1}{dt} = \frac{dy}{dt} = x_2, \quad \frac{dx_2}{dt} = \frac{d^2y}{dt^2} = x_3, \quad \frac{dx_3}{dt} = \frac{d^3y}{dt^3}$$

and

$$\frac{d\boldsymbol{X}}{dt} = \boldsymbol{A}\,\boldsymbol{X} + \boldsymbol{b}\,u$$

$$y = [\,1 \quad 0 \quad 0\,]\,\boldsymbol{X} = \boldsymbol{c}^T\boldsymbol{X}$$

Let the control law be

$$u = r - \boldsymbol{k}^T\boldsymbol{X}$$

$$\text{where } \boldsymbol{k}^T = [\,k_1 \quad k_2 \quad k_3\,]$$

Consider

$$H(s) = \frac{k^T X(s)}{Y(s)} = \frac{k^T X}{c^T X}$$

$$= \frac{k_1 x_1 + k_2 x_2 + k_3 x_3}{x_1}$$

$$H(s) = \frac{k_1 x_1 + k_2 s x_1 + k_3 s^2 x_1}{x_1}$$

$$= k_1 + s k_2 + s^2 k_3$$

$$\therefore G H = \frac{c_o (k_1 + s k_2 s^2 k_3)}{s^3 + a_2 s^2 + a_1 s + a_0}$$

and the overall transfer function is

$$\frac{Y(s)}{R(s)} = \frac{G}{1 + G H} = \frac{c_0}{(s^3 + a_2 s^2 + a_1 s + a_0) + c_0 (k_3 s^3 + k_2 s + k_1)}$$

$$= \frac{c_0}{s^3 + (a_2 + c_0 k_3) s^2 + (a_1 + c_0 k_2) s + (a_0 + c_0 k_1)}$$

using the final value theorem,

$$\lim_{t \to \infty} y(t) := y_{ss} = \lim_{s \to 0} s\, Y(s)$$

$$\therefore y_{ss}(t) = \lim_{s \to 0} \frac{s\, c_0\, R(s)}{s^3 + (a_2 + c_0 k_3) s^2 + (a_1 + c_0 k_2) + (a_0 + c_0 k_1)}$$

for step input $R(s) = s^{-1}$

$$\therefore \; y_{ss} = \frac{c_0}{a_0 + c_0 k_1} := 1 \; \textit{for zero error}$$

$$ie, \quad k_1 = 1 - \frac{a_0}{c_0}$$

which is fixed. By appropriate selecting the value of k^T, we can implement any desired characteristic equation as we want.

observer design

original plant:

$$\frac{d\underline{X}}{dt} = \underline{A}\,\underline{X} + \underline{b}\,u$$

$$y = \underline{c}^T \underline{X}$$

Let $\hat{\underline{X}}$ be the estimated state vector.

Let

$$\frac{d\hat{X}}{dt} = A\hat{X} + b\,u + L\,(y - \hat{y})$$

$$\hat{y} = c^T \hat{X}$$

where L is the observer matrix

$$L = [\, l_1 \;\; l_2 \;\; l_3 \,]$$

define $e = X - \hat{X}$

$$\rightarrow \frac{de}{dt} = \frac{dX}{dt} - \frac{d\hat{X}}{dt}$$

$$= A\,X + b\,u - (\,A\hat{X} + b\,u + L\,(\,c^T X - c^T \hat{X})\,)$$

$$= A(\,X - \hat{X}\,) - L\,c^T(\,X - \hat{X}\,)$$

$$= (\,A - L\,c^T\,)\,e$$

By appropriate selecting the eigenvalues of e, the error of the estimated state vector will died out very quick. A state diagram is shown in figure 20.

figure 20.

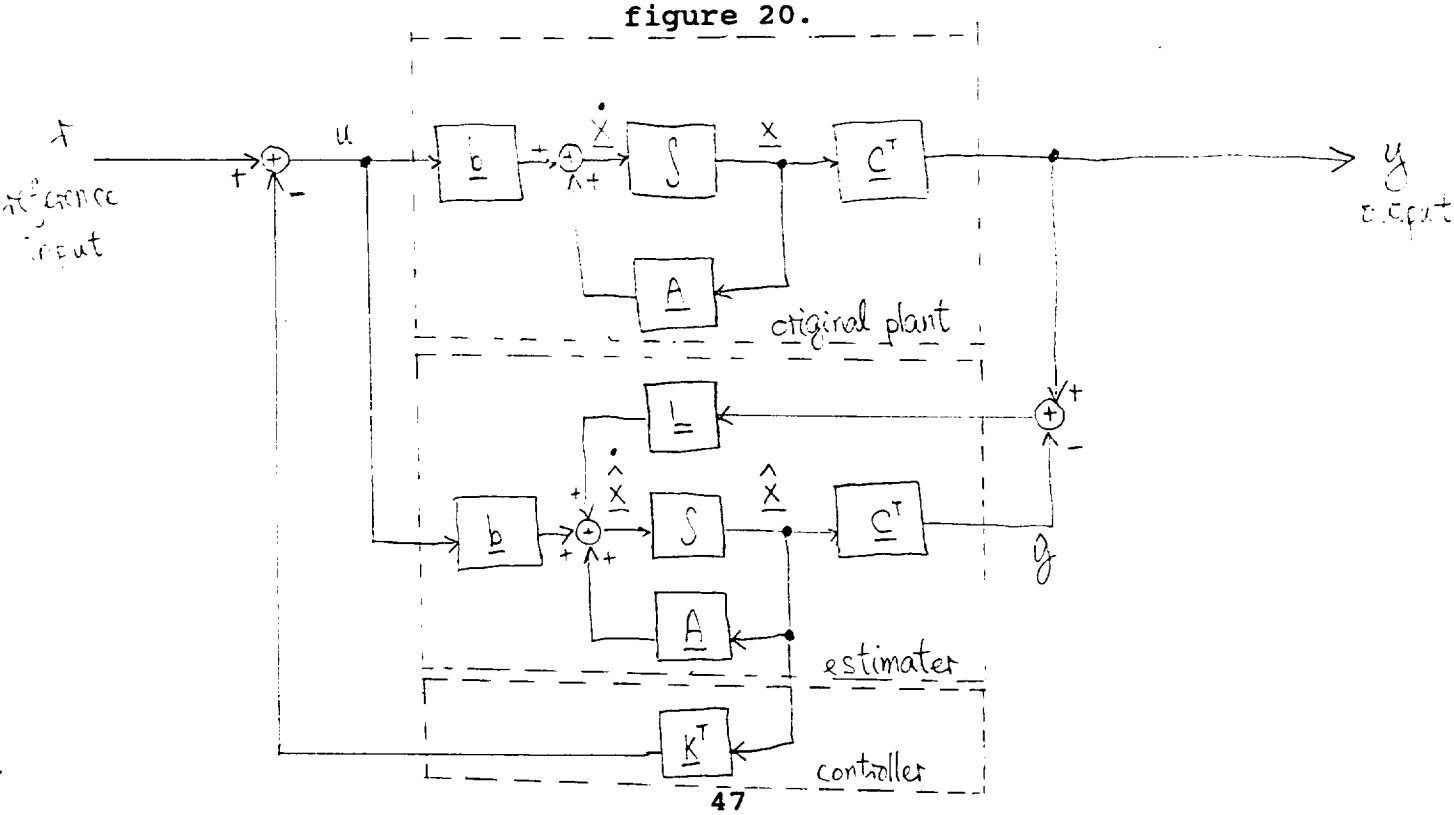

Appendix IV

Computer codes for nonlinear plant dynamics

```
{$N+,E+}
program project(outputo);        {3\21\1993}
  var
    d:char;
    i, j, n, nstep, e, b:integer;
    h, h2, X1max, X4max, t, r, u, dum:real;
    k:array[1..3] of real;
    x,y:array[1..2,1..4] of real;
    f:array[1..4,1..4] of real;
    outputo:text;
  { This is a Runge-Kntta method of order 4. }
  procedure initizing;
    begin
      t:=0;                  {initial time}
      h:=1/1024;             {incremental time step}
      n:=4;                  {number of equations}
      for i:=1 to 2 do       {initial value}
       for j:=1 to 4 do
        begin
        x[i,j]:=0;
        y[i,j]:=0;
        end;
      for i:=1 to 4 do
       for j:=1 to 4 do
```

```
        f[i,j]:=0;
      nstep:=4096;       {number of step}
      r:=1;
      k[1]:=1.01;
      k[2]:=0.021561;
      k[3]:=0.0001505;
    end;

  procedure get_value_f;
    begin
     f[e,1] := x[b,2];
     f[e,2] := (382.3996e-6)*(4.3434e-3 +
               x[b,1]*x[b,3])*(0.00762*x[b,3] +
               0.57*x[b,1])/(sqr(sqr(0.00762) - sqr(x[b,1])));
       dum  := (y[b,2] - x[b,2])/h; {estimated the second derivate}
         u    :=    r  -  (k[1]*x[b,1]  +  k[2]*x[b,2]  +  k[3]*dum);
{control law}
     f[e,3] := -44.2995*x[b,3] + 5.5374*u;
     f[e,4] := 1;        { x[4]= time }
    end;

  procedure RK4SYS;
     begin
        h2:=0.5*h;
        for j:=0 to nstep do
           begin
```

```
                for e:=1 to 2 do
                begin
                  b:=e;
                  get_value_f;
                  for i:=1 to n do
                    x[2,i]:=x[1,i] + h2*f[e,i];
                end;
                e:=3;
                get_value_f;  {get f3}
                for i:=1 to n do
                  x[2,i]:=x[1,i] +h*f[e,i];
                e:=4;
                get_value_f;  {get f4}
                y[1,2]:=x[1,2];
                y[2,2]:=x[2,2];
                for i:=1 to n-1 do {compute next x(t+h)}

x[1,i]:=x[1,i]+h*(f[1,i]+2*(f[2,i]+f[3,i])+f[4,i])/6;
                x[1,4]:= t+j*h; {advance solution}
                if j mod 64 =0 then  {write the result}
                begin
                  for i:=1 to n do
                  write(outputo,x[1,i],',');
                  writeln(outputo);
                  writeln(x[1,1],',',x[1,4]);
                end{if loop}
```

```
    end;{for j loop}
end;{RK4SYS}

begin {main}
   assign(outputo,'a:\p1.dat');
   rewrite(outputo);
   writeln(outputo);
   initizing;
   repeat
   RK4SYS;
   write('want change Y/N ?');
   readln(d);
   if d='y' then
    begin
     writeln('k1=',k[1],' k2=',k[2],' k3=',k[3]);
     write(' enter k1,k2,k3');
     readln(k[1],k[2],k[3]);
    end;
   until (d<>'y');
   writeln(outputo, ' Job completed. ');
   writeln('  Job completed.');
   close(outputo);
end.
```